12 Atmospheric Propagation

Lead authors

Tony F. W. Embleton
National Research Council
Ottawa, Ontario, Canada

Gilles A. Daigle
National Research Council
Ottawa, Ontario, Canada

Introduction

How sound propagates from a source to a receiver outdoors is a complicated problem because there are several wave propagation and meteorological mechanisms that can affect the result. The shape and type of ground surface also play a part. The received signal is influenced by each mechanism in a different way and to an extent that depends on range, source and receiver heights, and sound frequency.

The study of sound propagation in the atmosphere has a long and interesting history (refs. 1 and 2). As early as 1636, Mersenne (1588–1648) measured the speed of sound by timing the interval between the flash and sound of a gun blast. He obtained a value of 230 toises per second, equivalent to about 448 m/sec. A contemporary, Gassendi (1592–1655) noted that the speed of sound was independent of its intensity, since the speed was the same whether the sound was made by a large weapon, such as a cannon, or a smaller one, such as a musket. Derham in 1708 concluded that favorable winds speeded sound propagation while adverse winds retarded it: he did not measure temperature but concluded that the speed of sound was the same in summer as in winter. In 1740, Bianconi in Bologna showed that the speed of sound definitely increased with increasing air temperature. The first precise measurements of the speed of sound were probably those made in 1738 under the direction of the Academy of Paris. When corrected to 0°C, the value obtained was 332 m/sec—within about 0.3 percent of the best modern value—and it was obtained two and a half centuries ago.

From about 1860 onward, there was considerable interest in fog signaling for ships—Joseph Henry in the United States and Tyndall in Britain investigated what we would today call absorption or scattering by water vapor. Stokes at that time in a private letter to Tyndall wrote that scattering was more likely caused by temperature differences in the air. Knowledge of sound propagation in the atmosphere has usually developed in response to the needs of practical problems. During the first World War there was the problem of locating artillery; in the 1930's, the need to understand the loss of brilliance of music in concert halls; in the 1960's, the concern over noise produced by many forms of new technology—intense like commercial jet aircraft or widespread like powered lawn mowers and air conditioning. Since then the increasing

numbers of noise sources, and often their greater intensity, have increased the social and political pressures on acousticians to yet again advance their knowledge of sound propagation outdoors. Significant progress has been made in recent years (refs. 3 and 4).

This chapter reviews the current state of knowledge of each basic mechanism and how each changes the spectral or temporal characteristics of the sound received at a distance from the source. An understanding of these mechanisms is important since some affect even short-range measurements, when one is often attempting to characterize the source. Long-range measurements or predictions, such as when one is attempting to predict the influence of a source on a neighboring community or to detect the source at the greatest possible range, are affected in different ways and by other mechanisms.

Some of the basic processes affecting sound wave propagation are present in any situation. These are

1. Geometrical spreading—Sound levels decrease with increasing distance from the source; there is no frequency dependence.
2. Molecular absorption—Sound energy is converted into heat as the sound wave propagates through the air; there is a strong dependence on frequency.
3. Turbulent scattering—Local variations in wind velocity and temperature induce fluctuations in phase and amplitude of the sound waves as they propagate through an inhomogeneous medium; there is a moderate dependence on frequency.

Other phenomena occur only because of the presence of the ground and are usually most significant near the ground. These phenomena and the features that cause them are

1. Reflection at the ground surface—The sound field reflected at the ground interferes with the direct sound field; interference is a repetitive function of frequency; height of source and receiver, their distance apart, and the type of ground surface are important parameters.
2. Type of ground surface—Surfaces have a finite and complex acoustic impedance that results in a phase change on reflection of a sound field and a reflection coefficient that is a function of angle of incidence; this in turn leads to the existence of a ground wave in addition to a plane reflected wave and under some circumstances, to a trapped surface wave.
3. Shape of ground surface—Concave ground surfaces can result in multiple ray paths between source and receiver and hence increased sound levels; convex ground surfaces such as berms or low hills can act as sound barriers and lead to an acoustical shadow that is penetrated by diffracted and scattered waves.
4. Near-surface micrometeorology—The ground surface heats (usually daytime) or cools (nighttime) relative to the atmosphere leading to vertical gradients in temperature; viscous drag of the surface on wind produces similar vertical gradients in wind speed; as a result, sound fields are refracted upward (warmer ground or upwind) or downward (cooler ground or downwind).

Finally, these phenomena depend for the most part on different parameters, and so each can be strong or weak depending on the particular circumstances. Furthermore the phenomena coexist, and a given sound field may be influenced by different

mechanisms at different frequencies, at different heights, or at different distances. These coexisting mechanisms sometimes reinforce, and sometimes nullify, each other.

Geometrical Spreading

Some energy spreads out as it propagates away from its source. At distances that are large compared with the effective size of the sound source, the sound wave fronts spread spherically in three dimensions provided that the atmosphere is isotropic. Note that sound does not necessarily radiate equally in all directions as it would from a true point source. However, if the point source approximation is applicable, the sound level decreases at the rate of 6 dB per doubling of distance. This situation exists once the directionality pattern of the source does not change as a function of distance. For coherent sources (those for which unique phase relationships exist between all the radiating elements), the Fresnel region near the source extends to a distance somewhat greater than the square of the source diameter, or square of its length, divided by the wavelength of the sound. Within this near-field region there is interference between coherent elements of the source and there are no simple relations between sound levels and position.

One should take care in defining the effective size of the source. For example, noise from an axial flow compressor is generated by flow past individual blades, but the pure-tone components of this noise are generated coherently by the complete annular ring of blades and are radiated from the inlet duct of the compressor (in some engines also from the fan outlet). The effective size of the source is the diameter of the inlet duct (or the distance between the inlet orifice and the fan outlet). When the noise source is a turbulent jet, the effective size of the source can be the whole mixing region, which is much larger than any dimension of the mechanical hardware.

The 6-dB decrease per doubling of distance relationship applies either to the instantaneous sound pressure level (or time-averaged sound level of a stationary source) or to the maximum sound pressure level reached during a passby of a moving source.

One must be careful to distinguish these from certain measures of total sound exposure received from a moving source during a passby event. Such measures as single event noise exposure level (SENEL) represent the total value of sound pressure squared when integrated throughout the passby event. In these cases, although the maximum sound pressure level decreases by 6 dB per doubling of the closest distance of approach, the length of time during which the sound pressure level is within a given difference from the maximum value also doubles, and the net result for any such time-and-intensity measures is that the level decreases at the rate of 3 dB per doubling of distance from the source. Three decibels per doubling of distance also represents cylindrical spreading of sound energy propagating away from a line source. Such a sound is that from the traffic flow along a busy road, where the individual vehicles are a line of discrete point sources each radiating sound incoherently with respect to the others.

The phenomenon of geometrical spreading, and the corresponding decrease in sound level with increasing distance from the source, is the same for all acoustic frequencies or wavelengths. Certain parameters of the atmosphere directly affect sound levels calculated from geometrical spreading, but these effects are very small and rarely, if ever, detectable. For example, gross changes in temperature (not to be

confused with transverse temperature gradients that produce refraction) change the speed of sound and hence the sound energy density and measured sound pressure levels. The sound level measured at the ground (temperature of 20°C) directly below an aircraft flying at an altitude where the temperature is −40°C is 0.5 dB less because of this 60°C temperature change than it would be if there were no temperature change. In addition, if the relative humidity was 100 percent, the sound pressure level at the ground would be decreased by a further 0.2 dB because of air density changes alone.

Molecular Absorption

In contrast to geometrical spreading, the absorption of sound energy by the atmosphere is a significant function of frequency, temperature, pressure, and humidity. Studies of molecular absorption have a history going back to the 19th century and continue even today. In this section we summarize the basic mechanisms by which acoustic energy is absorbed by the atmosphere, we discuss the current ANSI Standard for calculating atmospheric absorption (ref. 5), and finally we mention current research to improve the accuracy of the calculations.

The absorption of acoustic energy by a mixture of gases occurs through two basic physical mechanisms (ref. 6). The first involves the direct transfer of acoustic energy (ordered motion) into heat energy (random motion) through processes involving viscous effects and heat conduction. These two loss processes have been known since the 19th century and are known today as classical absorption. The second basic physical mechanism of absorption is molecular relaxation. The compressional energy of the acoustic wave is redistributed into rotational and vibrational modes of the molecules through binary collisions. The time lag associated with this transfer leads to absorption of sound energy, with maximum absorption (per wavelength) being reached at the relaxation frequency. For frequencies below 10 MHz, absorptions due to classical losses and molecular relaxation are additive. Current theory assumes that the total molecular absorption of acoustic energy by the atmosphere is the sum of four terms:

$$\alpha = \alpha_{cl} + \alpha_{rot} + \alpha_O + \alpha_N \tag{1}$$

where α_{cl} is the classical absorption, α_{rot} the absorption due to rotational relaxation, and α_O and α_N are, respectively, the absorption due to vibrational relaxations of oxygen and nitrogen.

The classical absorption is a function of temperature, pressure, and frequency. It is the dominant absorption mechanism for acoustic energy at high frequencies. The absorption due to rotational relaxation is also a function of temperature, pressure, and frequency. Furthermore, the rotational relaxation frequency in the atmosphere is well above 10 MHz. This permits the rotational absorption constant to be combined with the classical absorption constant into one expression for practical purposes. The combined expression yields the curve labeled "α_{cl+rot}" in figure 1. These two absorptions provide the dominant losses at frequencies above approximately 30 kHz.

Historically, classical absorption and rotational relaxation were by themselves unable to account for the loss of brilliance long observed in concert halls in the frequency range above about 2 kHz. In response to this, theory was developed in the early 1930's which included the contribution of the vibrational relaxation of oxygen.

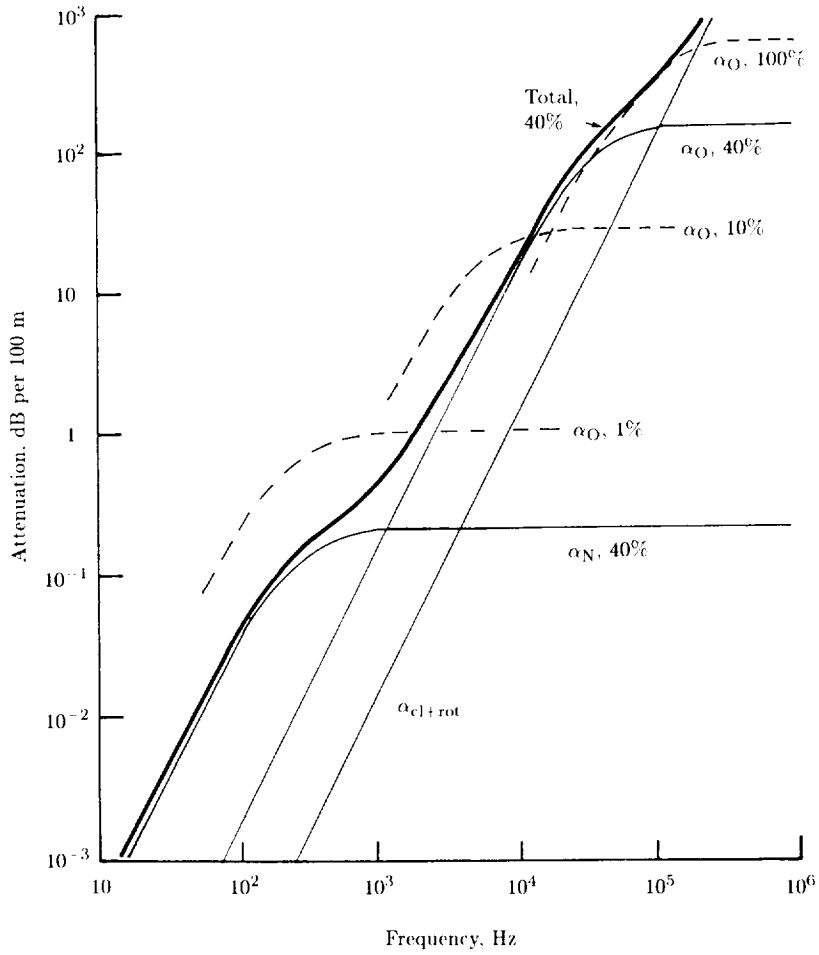

Figure 1. Decrease in sound pressure level with distance as a function of frequency due to four molecular processes in equation (1). Temperature, 20° C; pressure, 1 atm; relative humidity indicated in percent.

In addition to frequency, temperature, and pressure, the vibrational relaxation absorption depends strongly on the concentration of water vapor. Collisions with water vapor molecules speed the energy transfer process and hence influence the frequency of maximum absorption. The dashed curves labeled "α_O" in figure 1 indicate how the relaxation frequency, and hence the absorption due to the oxygen relaxation, changes at 20°C when the relative humidity increases from 1 to 100 percent. At normal temperatures and relative humidities, the oxygen relaxation provides maximum absorption at frequencies above about 2 kHz.

In the 1960's and early 1970's, increasing activity was devoted to predicting environmental noise in urban areas for community planning, including the control of aircraft noise. Measurements began to show deviations from the theory for molecular absorption at low frequencies, where most of the sound energy of environmental noise

is found. Initially empirical procedures (ref. 7) were developed to account for the discrepancies below 2 kHz. Later it was realized that the vibrational relaxation of nitrogen is the main absorption mechanism at low frequencies. The contribution to absorption of the nitrogen relaxation is illustrated by the curve labeled "α_N" in figure 1.

The total molecular absorption due to the four contributions in equation (1) is shown by the curve labeled "Total" in figure 1. The absorption is predicted for a pressure of 1 atm, temperature of 20°C, and relative humidity of 40 percent and is expressed in decibels per 100 m. For example, the total absorption under these conditions is about 1 dB/100 m at 2 kHz. A set of fairly simple equations for practical calculations of the four terms in equation (1) form the basis of an ANSI standard (1978) for atmospheric absorption (ref. 5). The scientific support and experimental evidence for this standard are found in reference 6. The accuracy of the atmospheric absorption calculated from this standard (ref. 5) is approximately 10 percent for temperature from 0° to 40°C, relative humidity from 10 to 100 percent, frequency from 50 Hz to 10 MHz, and atmospheric pressure less than 2 atm. The calculations can have an accuracy of 5 percent over a more limited range of variables within the ones quoted above. On the other hand, outside this quoted range, for example, at low frequencies and low humidities, the accuracy of the calculation is usually worse than 10 percent. There is still a need for more fundamental work, especially at the more extreme conditions, to increase the understanding of these processes. Some recent work (ref. 8) aimed at extending the measurements at low frequencies has revealed discrepancies in the accepted relaxation frequencies of oxygen. It is expected that this and other new knowledge will result in a revision of the current ANSI standard (1978).

Effects Due to the Presence of the Ground

In this section, we consider only the direct effects on sound propagation caused by the ground. These effects are additional to those of geometrical spreading and molecular absorption already discussed. We postpone until later any discussion of near-surface micrometeorological effects such as those caused by heating or cooling. Propagation effects caused by the ground are most significant within a few wavelengths, that is, only a few meters above the ground surface. Furthermore, the ground has a greater effect on sound waves traveling essentially horizontally just above the ground than it does on sound waves impinging from nearly vertical directions.

When the sound source and receiver are above a large flat ground, sound reaches the receiver via two paths: directly from the source to the receiver, the direct field, and after being reflected from the ground surface between the source and receiver, the reflected field (fig. 2). Most ground surfaces are porous to some degree and therefore their acoustic impedance is complex. In simple terms, one may think of a resistive component of impedance that describes the losses of sound energy due to thermal and viscous effects in the interstices of the ground material; there is also a reactive component due to flow into and out of the porous ground in response to the alternating acoustic pressure in the air just above the surface that results in compression either of gas in the interstices or of the solid itself. The complex acoustic impedance of the ground is associated with a complex reflection coefficient

that is rarely as large as unity and is a function of angle of incidence. The sound field reflected from the surface therefore suffers (1) a reduction in amplitude and (2) a phase change between zero and π radians (0° to 180°). There is another more subtle, but very important, effect on the sound field: if the incident waves are plane, the reflected waves are also plane because all parts arrive with the same angle of incidence; but if the incident field is of some other shape (e.g., spherical), then different parts of the wave front meet the plane surface with different angles of incidence and are subjected to reflection coefficients that differ in magnitude and phase. Thus the reflected field has a different shape; for example, a spherical field no longer appears to come from a point source below the surface. Instead the source region becomes blurred and theoretically stretches to infinity.

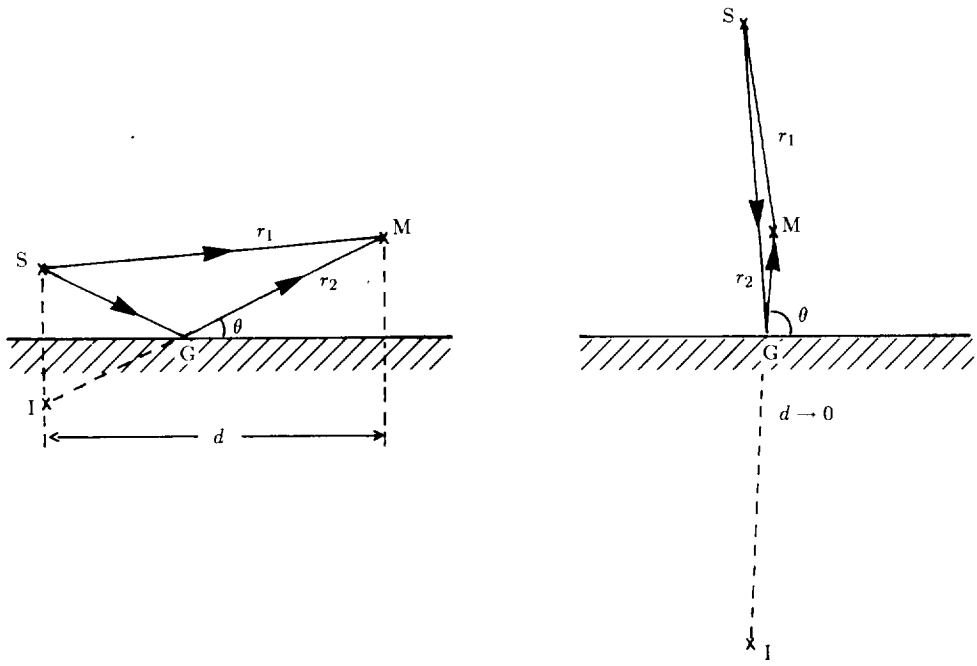

(a) Source near the ground. *(b) Source nearly overhead.*

Figure 2. Schematic of the direct sound field by the ray path SM and that reflected at the ground surface by the path SGM. (I is the location of the geometric image of the source in the ground.)

Plane Waves

The reflection coefficient R_p for plane waves incident on a plane surface is given in its simplest form by

$$R_p = \frac{\sin\theta - Z_1/Z_2}{\sin\theta + Z_1/Z_2} \tag{2}$$

where θ is the angle of incidence (fig. 2) and Z_1/Z_2 is the ratio of the characteristic impedance of air at ground level to the specific normal acoustic impedance of the

ground surface. The impedance Z_2 is complex. This simple form of the equation for the complex reflection coefficient R_p is for a ground surface of local reaction, that is, a surface whose reflection coefficient at any point is not significantly affected by the sound field incident at neighboring points. If the ground can support a significant amount of wave propagation, either in the solid material or in the air of the pores, then the expression for the reflection coefficient becomes more complicated, but its properties remain almost the same. In practice the impedance Z_2 must always remain finite, even though it is very large for hard surfaces such as concrete, so that for θ small enough to make $\sin\theta << |Z_1/Z_2|$, R_p always approaches -1 at grazing incidence. Figure 3 shows the magnitude $|R_p|$ and phase change ϕ of the complex reflection coefficient $R_p = |R_p|e^{i\phi}$ for plane waves incident on a typical grass-covered surface such as an airport or field. Only at grazing incidence does the magnitude of the reflection coefficient reach unity, and this is accompanied by a phase change on reflection of π radians (180°). For most angles of incidence that are not close to grazing, the magnitude of the reflection coefficient is between 0.5 and 1.0, and the phase change on reflection of the sound waves is less than about $\pi/4$ radians (45°) and can often be ignored. The general features shown in figure 3 apply for all ground surfaces although the angle of incidence scale (abscissa) and the magnitude of the reflection coefficient scale (ordinate) change depending on the acoustic impedance of the ground surface. For example, the magnitude of the reflection coefficient $|R_p|$ always has a minimum when its phase change is $\pi/2$ radians (90°). The angle of incidence for which this occurs becomes more nearly grazing as the acoustic impedance of the ground increases, for surfaces like concrete, asphalt, or packed earth, and becomes more oblique as impedance decreases, for softer ground surfaces like snow or the ground in a forest.

Ground and Surface Waves

Because the magnitude and phase of the reflection coefficient R_p vary with angle of incidence, as shown in figure 3, the total sound field near the ground cannot usually be described mathematically by the simple addition of two terms, the incident sound field and the reflected sound field multiplied by the plane-wave reflection coefficient of equation (2). An additional term is required that allows, in effect, for the fact that each curve in figure 3 is not a horizontal straight line. A more complete expression for the sound pressure p, borrowed from electromagnetic theory and known as the Weyl–Van der Pol solution is

$$\frac{p}{p_o} = \frac{e^{ikr_1}}{kr_1} + R_p\frac{e^{ikr_2}}{kr_2} + (1 - R_p)F\frac{e^{ikr_2}}{kr_2} \tag{3}$$

In equation (3), p_o is a constant, k is the wave number of the sound field (the number of wavelengths in a length of 2π meters), r_1 and r_2 are the ray paths in figure 2, and F is a complex amplitude function (ref. 9) that allows for the curvature of the incident sound field and, under some circumstances, the possible existence of a surface wave. Mathematically F is related to the complex error function of a parameter w, known

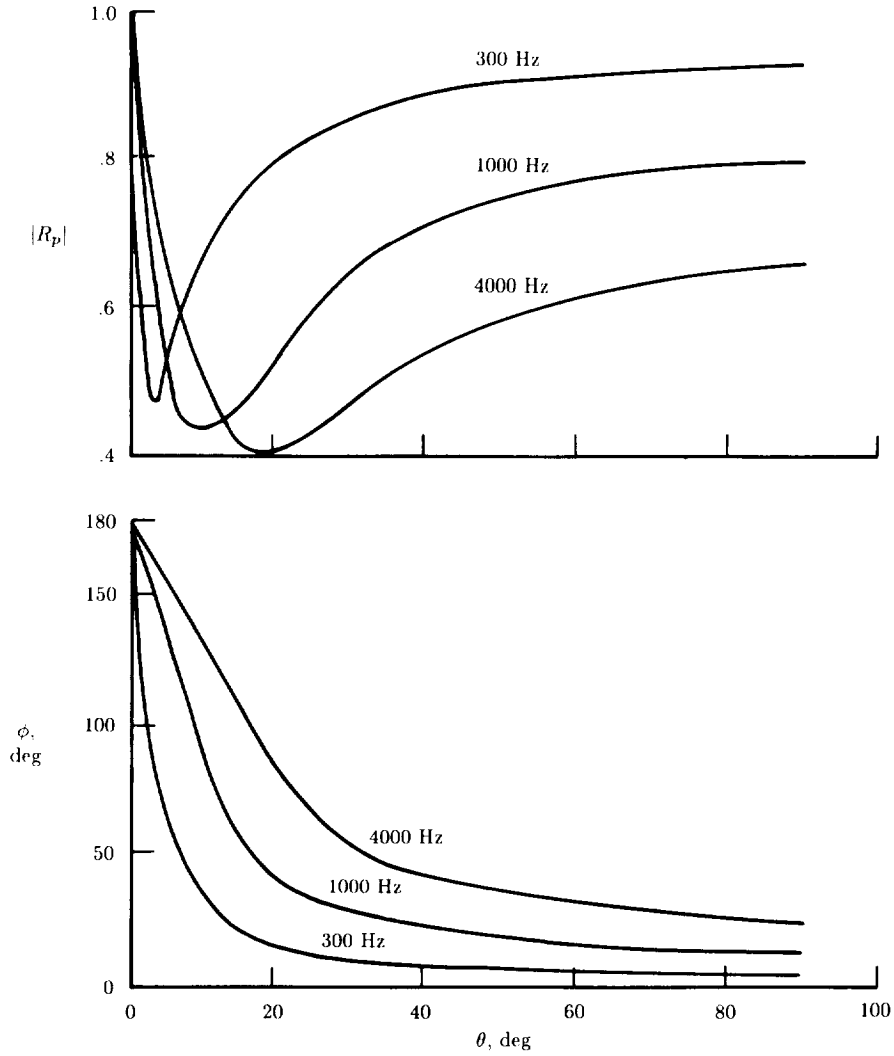

Figure 3. The magnitude $|R_p|$ and phase change ϕ of the plane-wave reflection coefficient as a function of angle of incidence θ at three typical frequencies for a grass-covered surface.

in this context as the numerical distance, and given by

$$w = \left(\frac{1}{2}ikr_2\right)\left(\sin\theta + \frac{Z_1}{Z_2}\right)^2 \tag{4}$$

The first term on the right side of equation (3) clearly represents the direct sound field in both phase and amplitude, the second term represents the field reflected at the ground surface but assuming the plane-wave reflection coefficient at the angle of specular reflection, and the third term corrects the reflected field to account for

the angle of reflection systematically varying with position along the surface. This third term in equation (3) is called a ground wave in acoustics but may also include a surface wave under some circumstances (beware that the term "ground wave" in electromagnetic propagation applies to the whole right side of eq. (3)).

When the source and receiver are both relatively near the ground and are a large distance apart, the direct and reflected fields (the ray paths r_1 and r_2 in fig. 2(a)) become nearly equal and the grazing angle θ tends to zero. The direct and reflected sound fields then cancel each other because $R_p \rightarrow -1$, and any sound reaching the receiver (apart from mechanisms to be described later) is explained theoretically by this third term of equation (3).

The amplitude factor F is shown in figure 4 vs. the numerical distance w described by equation (4). The factor F is complex and is shown for several values of the phase angle ψ of the ground impedance,

$$\psi = \tan^{-1}\left(\frac{\text{Im } Z_2}{\text{Re } Z_2}\right) \tag{5}$$

It is intuitively useful to consider the abscissa of figure 4, the numerical distance w, as the propagation distance between source and receiver but scaled for the value of frequency (proportional to k), for impedance Z_1/Z_2, and for angle of incidence θ. The behavior of the ground wave during propagation is best described by assuming for the moment that the ground surface is purely resistive, that is, the curve for $\psi = 0°$ in figure 4. This curve cannot contain any surface waves (see below). Then at short distances $w << 1$, the ground wave suffers no excess attenuation, $|F|$ is essentially unity, and the second and third terms of equation (3) combine to describe a sound field as if it were reflected from an infinitely hard surface. At greater distances $w >> 1$, or equivalently at higher frequencies, the ground wave decreases at a rate that is 6 dB per doubling of distance faster than that due to geometrical spreading alone.

In reality the phase angle ψ of the ground impedance is about 45° for grass-covered and most other ground surfaces at least up to frequencies of a few kilohertz. The curve for $\psi = 45°$ in figure 4 shows a substantial increase in $|F|$, especially for numerical distances slightly greater than unity. This increase in $|F|$ occurs only for positive values of ψ, which in turn are related to the porous or capacitive behavior of ground surfaces for acoustic waves. The increase is due to the existence of a surface wave which is coupled to the ground but propagates in the air with an amplitude that has a maximum at the ground surface and decreases exponentially with height. For those whose experience and intuition are more mathematical than experimental, the ground wave corresponds to a branch line integral, and the surface wave to a pole. Thus, for certain values of complex impedance, the third term in equation (3) is given completely by a branch line integral, but as impedance is varied, it may become necessary to allow for the contribution from a pole. In these cases the pole contribution effectively appears to grow out of the contribution from the branch line integral, just as the surface wave appears out of the ground wave when the values of complex surface impedance allow.

Obviously ground and surface waves are closely related but their fundamental origins differ, as does their behavior during propagation. Ground waves exist because curved wave fronts strike different parts of the ground at different angles of incidence

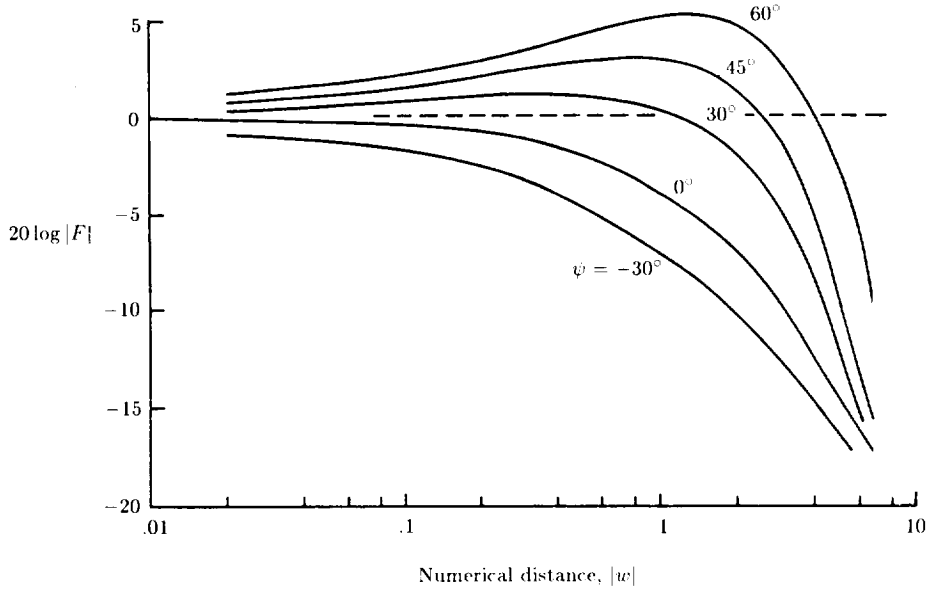

Figure 4. The magnitude of the complex amplitude factor F in decibels as a function of numerical distance w (eq. (4)). (From ref. 3; see also ref. 9.)

and because the reflection coefficient of finite-impedance ground is also a function of angle of incidence. Ground waves exist unless the ground is infinitely hard or infinitely soft or unless the incident wave fronts are plane, that is, the source can be considered infinitely far away. Surface waves exist when the ground surface is sufficiently porous, relative to its acoustical resistance, that it can influence the airborne particle velocity near the surface and reduce the phase velocity of sound waves in air at the surface. This traps some of the sound energy in the air, regardless of the shape of the incident sound field, to remain near the surface as it propagates from the source to the receiver. This latter point may be significant because surface waves, which spread cylindrically (in horizontal directions only), decrease at 3 dB per doubling of distance, whereas all other components of the sound field, including the ground wave component of the reflected sound field, decrease by at least 6 dB per doubling of distance. Though surface waves may initially decrease more slowly with distance, they eventually decay rapidly relative to other components of the total sound field because they are closely coupled to the ground surface and lose energy exponentially with distance through viscous and thermal processes in the pores of the ground.

Acoustic Impedance of Ground Surfaces

Sound waves incident on a ground surface are reflected and interfere with the incident field. This interference field can be probed within a few wavelengths of the ground to measure sound pressure and phase, or equivalently the position of maxima and minima of pressure, or to measure the distribution of phase gradient or of phase, in order to determine the reflection coefficient R_p. Alternatively the ground

impedance can be found directly by determining the pressure and the particle velocity at the surface. All these measurements are difficult to make with the necessary accuracy for most ground surfaces, and so various techniques have been used, each of which provides results of sufficient accuracy over a different but limited range of frequencies or values of ground impedance. Anybody planning to undertake such measurements is strongly advised to read the original papers so as to be aware of the subtleties of the various techniques and precautions that are important to obtaining valid results. We shall do no more than outline each of the measurement techniques and indicate their principal strengths and limitations.

Some early values of ground impedance were measured in reference 10 with an impedance tube "screwed" into the ground in situ to a depth of about 0.2 m. Like several of the other techniques to be mentioned, these measurements are restricted to normal incidence, suffer from the uncertainty of knowing exactly where the theoretical ground surface is located, and can change the flow resistivity, porosity, or other parameters of the microstructure of the ground surface. To avoid some of these limitations, Dickinson and Doak developed a technique based on measuring the pressure profile along a line perpendicular to the surface below a loudspeaker suspended several meters above the surface—the ground surface remained undisturbed and the sound field was unconfined. Later the interference between the direct and reflected sound fields was measured (ref. 11) by moving a microphone along an inclined path, GM in figure 2(a). This method allowed measurements at oblique angles of incidence more appropriate to sound sources near the ground but were restricted to frequencies greater than about 400 Hz, that is, to wavelengths less than about 0.8 m, because the distance between interference minima is increased (inversely as $\sin\theta$) and becomes very large near grazing angles of incidence. More recently, a direct pressure vs. velocity, and hence impedance, measurement (ref. 12) has been obtained with a Helmholtz resonator, one side of the volume of the resonator being open and capable of being pushed into the ground surface. A motor-driven mechanical source provides a known volume velocity source and a microphone measures the resulting pressure. This technique is restricted to frequencies below about 300 Hz both by the capabilities of the sound source and by the requirement that the sound wavelength be large compared with the dimensions of the resonator. Another technique that measures both pressure and pressure difference near the surface, and hence by calculation the impedance at the surface, has been used in reference 13 for small areas of sound absorbent materials. Because of instrumental limitations and finite difference approximations, this technique allows sufficiently precise measurements only for frequencies greater than about 500 Hz. Still more recently, a two-microphone technique (ref. 14) has been used to measure pressure, phase, and phase difference along a vertical line in the spherically spreading interference field below a source suspended several meters above the ground. Measurements have been made down to 30 Hz over grass-covered ground.

A limited selection of measured values of the resistive and reactive components of normalized specific normal impedance for grass-covered ground at different sites is shown by the dashed curves in figure 5.

For many practical purposes our interest in the ground surface is merely the effect it has on the sound field in the air above it. The direct effect is through the reflection coefficient R_p that varies in the complicated way illustrated in figure 3 as a function

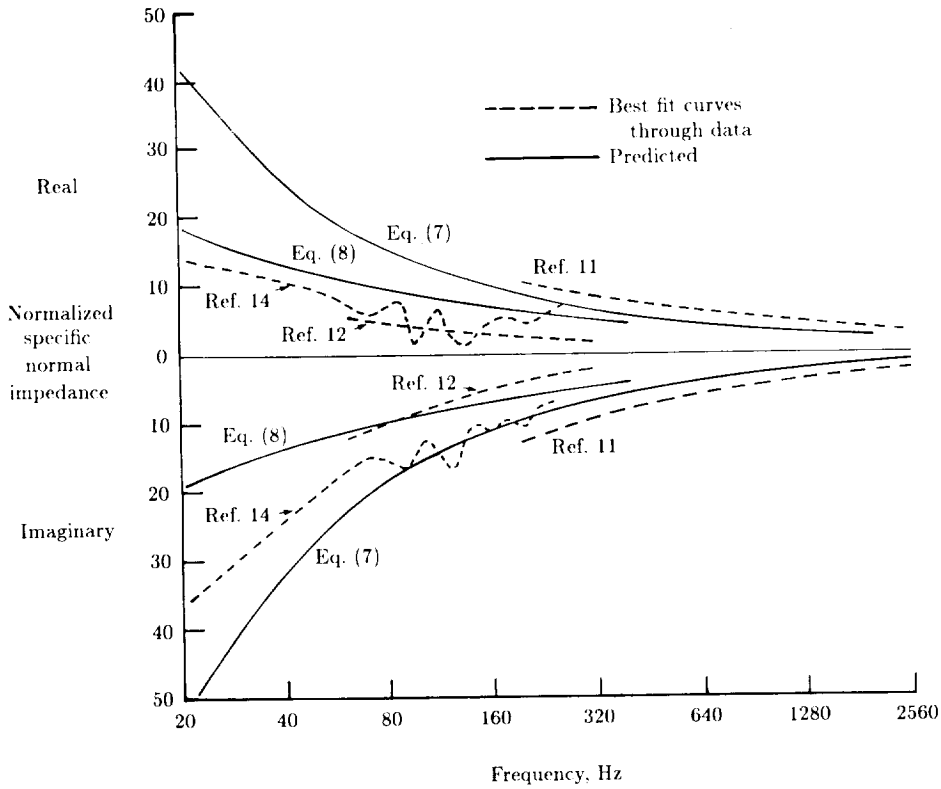

Figure 5. Normalized resistive (real) and reactive (imaginary) components of specific normal impedance for grass-covered grounds as a function of frequency. $\sigma_e = 150 \times 10^3$ Pa-sec/m^2 assumed in equations (7) and (8).

of angle of incidence and frequency. A simpler characterization of the ground is its specific normal acoustic impedance, Z_2 in equation (2). The impedance Z_2 is complex:

$$Z_2 = R_2 + iX_2 \tag{6}$$

where R_2 is the resistive component of the ground impedance, and X_2 its reactive component. Most ground materials are porous, and thus for nonlayered grounds the specific normal acoustic reactance of the surface is capacitive, or springlike in electrical or mechanical analogs. The impedance Z_2 is a function of frequency and its two components for typical grass surfaces are shown in figure 5. Such impedance curves were shown in reference 15 to be described for most porous ground surfaces by a single parameter, the effective flow resistivity σ_e of the ground. In reference 15 the empirical expressions earlier given in reference 16 were used for the specific acoustic impedance of fibrous porous materials. When the implied time dependence is $\exp(-i\omega t)$, these equations become

$$\frac{Z_2}{Z_1} = 1 + 0.051\left(\frac{f}{\sigma_e}\right)^{-0.75} + i0.0769\left(\frac{f}{\sigma_e}\right)^{-0.73} \tag{7}$$

Table 1. Ranges of Effective Flow Resistivity for Various Ground Surfaces

Type of surface	Flow resistivity, Pa-sec/m^2
0.1 m of new fallen, dry snow	7 to 30 $\times$ 10^3
Sugar snow	25 to 50 $\times$ 10^3
Forest floor, pine or hemlock	20 to 80 $\times$ 10^3
Grass on airfield, rough pasture	150 to 300 $\times$ 10^3
Rough roadside dirt, assorted particle sizes	300 to 800 $\times$ 10^3
Sandy silt, packed	0.8 to 2.5 $\times$ 10^6
Limestone chips, thick layer (0.01 to 0.025 m mesh)	1.5 to 4 $\times$ 10^6
Old dirt roadway, stones (0.05 m mesh), interstices filled	2 to 4 $\times$ 10^6
Earth, little vegetation and rain-packed	4 to 8 $\times$ 10^6
New asphalt, depending on particle size	5 to 15 $\times$ 10^6
Quarry dust, packed by vehicles	5 to 20 $\times$ 10^6
Old asphalt, sealed by dust and use	25 to 30 $\times$ 10^6
Concrete, depending on surface finish	30 to 100 $\times$ 10^6

where f is the frequency in hertz, $\omega = 2\pi f$, and σ_e is the effective flow resistivity of the ground in Pa-sec/m^2. Equation (7) is valid for a wide range of ground surfaces but tends to overestimate both components of the impedance below about 200 Hz. Table 1 gives the values of effective flow resistivity for various ground surfaces (ref. 17) that can be used in equation (7) to provide the specific normal acoustic impedance Z_2. This in turn can be used in equation (2) to provide the complex reflection coefficient R_p and, with figure 4, a complete description of the effect of the ground on the sound field above it.

The predicted effect of four ground surfaces on the spectrum of a sound wave measured 1.22 m above the ground at a distance of 500 m is shown in figure 6. In figure 6(a) the source is 2 m above the ground (i.e., nearly horizontal propagation) as in figure 2(a) and in figure 6(b) the source is essentially overhead as in figure 2(b). The flow resistivity parameters of the four curves correspond roughly to snow, grass-covered earth, packed earth, and concrete. The predominant feature of each curve in figure 6(a) is the broad minimum of sound pressure level in the range of frequencies from about 100 to 400 Hz over snow to around 4000 Hz over concrete. The shape is determined by the large phase changes on reflection at nearly grazing incidence, illustrated in figure 3, interacting with the phase differences as a function of frequency that occur because of path length differences between the direct and ground-reflected sound fields (fig. 2). In figure 6(b) for nearly perpendicular reflection at the ground surface, there is almost no phase change on reflection regardless of the effective flow

resistivity of the ground surface. The shape of the curves therefore differs very little between surfaces and is determined almost entirely by path length differences. The first minimum occurs at about 70 Hz, for which the receiver is at a height of one-quarter wavelength above the ground (i.e., the reflected field travels an extra half-wavelength compared with the direct field). Subsequent minima occur at 3, 5, 7, ... times 70 Hz.

It is convenient to be able to characterize a wide range of common ground surfaces by the value of one parameter, whether selected from table 1 or measured for a specific surface of interest. When the one-parameter model is not sufficiently precise, for example, at frequencies below about 200 Hz, or when the ground changes significantly near its surface or is noticeably layered, then more elaborate theory can be invoked. In reference 18 the acoustical properties of homogeneous and isotropic porous soils were shown to depend on four material parameters: flow resistivity, porosity, grain shape factor, and pore shape factor ratio. Of these parameters, the flow resistivity σ and porosity Ω are the two most important; furthermore, the empirically determined effective flow resistivity σ_e of the one-parameter model (eq. (7) and table 1) is essentially given by the product $\sigma\Omega$. Though in general more complicated, the four-parameter model yields a low-frequency and high-flow-resistivity approximation that provides better agreement with measured impedances at frequencies below 200 Hz than does the one-parameter model (eq. (7)). The normalized surface impedance derived from the four-parameter theory but limited to large values of the effective flow resistivity σ_e and low frequencies is (eq. (14) of ref. 18):

$$\frac{Z_2}{Z_1} = 0.218\left(\frac{\sigma_e}{f}\right)^{1/2}(1+i) \tag{8}$$

Equation (8) is an alternative to equation (7) and differs from equation (7) by predicting that the resistive and reactive components of the ground impedance are equal and vary as the inverse square root of the frequency. (Equation (7) predicts a variation close to the inverse three-quarter power of frequency.)

This same low-frequency, high-flow-resistivity approximation also provides an expression for the normalized surface impedance of a ground whose porosity decreases with depth (eq. (31) of ref. 18):

$$\frac{Z_2}{Z_1} = 0.218\left(\frac{\sigma_e}{f}\right)^{1/2} + i\left[0.218\left(\frac{\sigma_e}{f}\right)^{1/2} + 9.74\left(\frac{\alpha_e}{f}\right)\right] \tag{9}$$

Note that equation (9) is the same as equation (8) with the addition to the reactance of a term in α_e/f, where α_e is an effective rate of decrease in porosity with depth. It is predicted that the resistive component of the ground impedance is unchanged by the rate of change of porosity below the surface.

When the ground consists of a porous layer backed by an essentially rigid impervious base, the obvious additional parameter needed to describe the normal surface impedance is the layer thickness ℓ. The impedance of the surface layer Z/ℓ is then calculated by

$$\frac{Z_\ell}{Z_1} = \frac{Z_2}{Z_1}\coth\left(-ik_2\frac{\omega}{c_o}\ell\right) \tag{10}$$

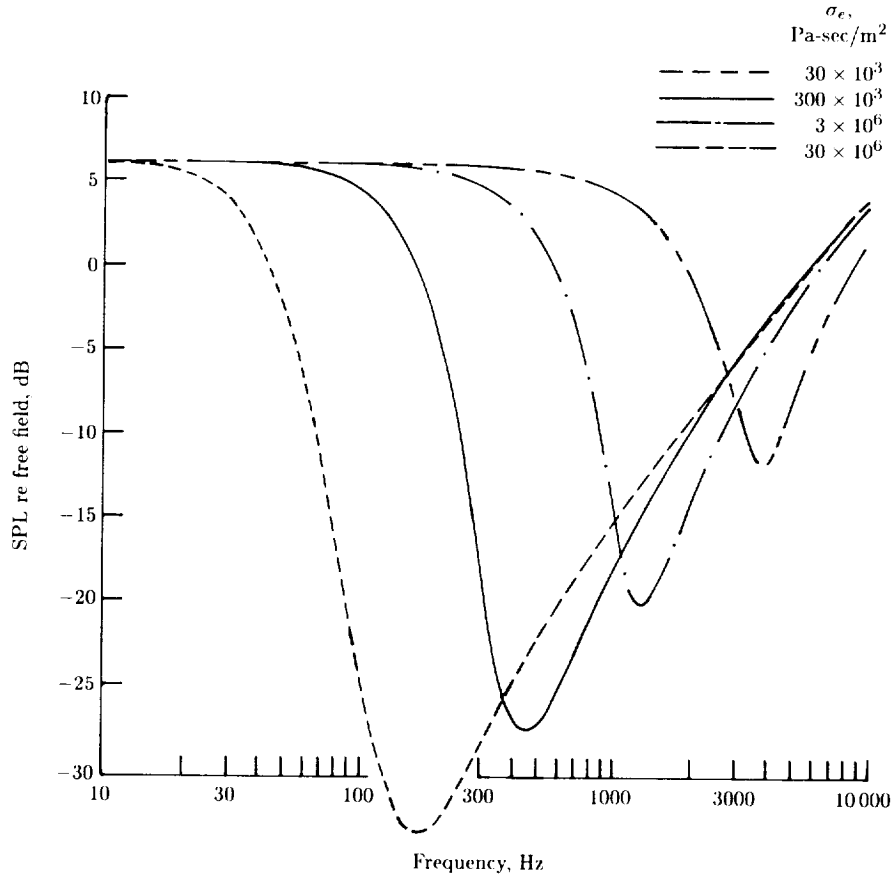

(a) Source 2 m above ground.

Figure 6. Predicted transmission spectrum measured 1.22 m above the ground for a source 500 m away.

where c_o is the sound speed at the surface of the ground and the normalized wave number k_2 is given by

$$k_2 = 1 + 0.0978 \left(\frac{f}{\sigma_e}\right)^{-0.693} + i0.189 \left(\frac{f}{\sigma_e}\right)^{-0.62} \tag{11}$$

and Z_2/Z_1 is given by equation (7), or equation (8) if appropriate.

The low-frequency, high-flow-resistivity approximation allows simplification of the expression for the surface impedance of a layered surface (ref. 18). At low frequencies, for many ground surfaces but not for a layer of snow because its flow resistivity is too small, equations (10) and (11) can be replaced by (eq. (33) of ref. 18):

$$\frac{Z_\ell}{Z_1} = 0.00082\, \sigma_e \ell_e + \frac{i38.99}{f\ell_e} \tag{12}$$

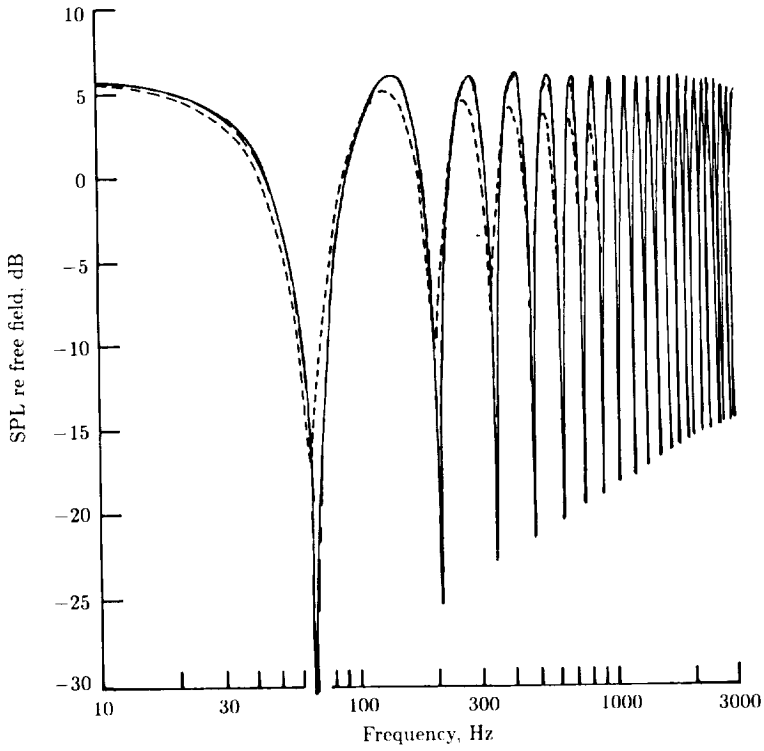

(b) Source directly overhead.

Figure 6. Concluded.

where ℓ_e represents the effective thickness of the layer given by $\Omega\ell$. The porosity for many ground materials lies in the range $0.3 < \Omega < 0.6$. Equation (12) shows that the normalized resistance of a surface layer backed by a hard rigid material is independent of frequency and that its normalized reactance increases rapidly with decreasing frequency.

The general effects on the sound field resulting from reflection at a layered surface for nearly grazing angles of incidence are illustrated in figure 7 (ref. 19). These sound pressure levels were measured at short range over a layered ground model of reticulated foam backed by a hard concrete floor. The principal effect is to deepen the minimum in sound pressure level in the so-called ground effect dip, in the region from 300 to 2000 Hz, compared with propagation over an infinitely thick layer of the same surface material. Although shown in these results, the minimum in sound pressure level does not necessarily occur at a higher frequency above a layered medium than above an infinitely thick ground.

Ground Surfaces With a Discontinuity of Impedance

As is apparent in figure 6(b), all types of ground have essentially the same effect on sound fields reflected almost perpendicularly to the surface. Different types of ground do however have different effects (fig. 6(a)) on sound traveling at nearly grazing angles

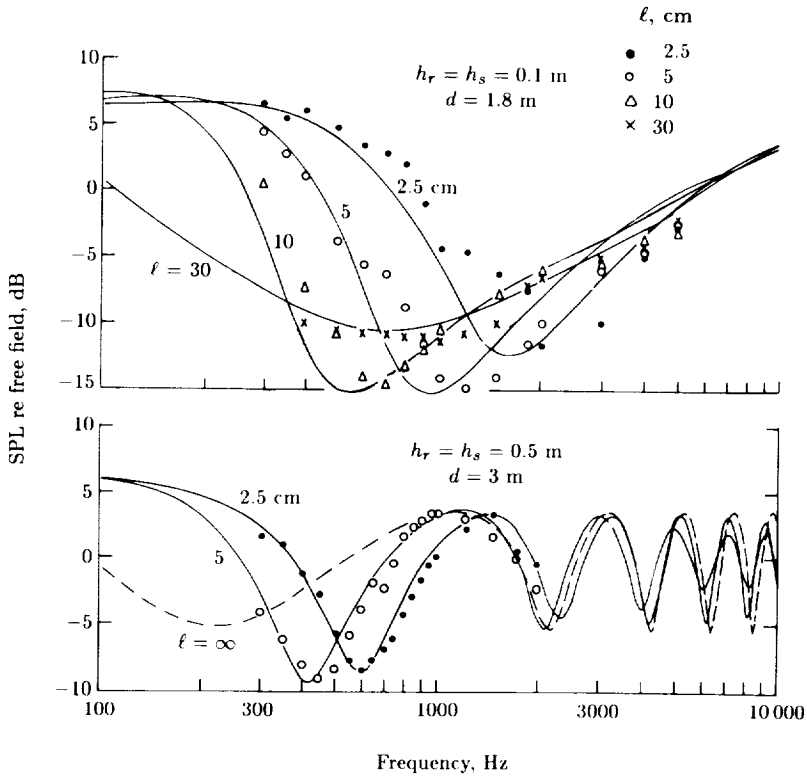

Figure 7. Comparison of sound pressure levels measured above layers of reticulated foam (data points) with predictions from equation (10)(curves).

of incidence. This latter configuration is of importance in many practical situations, for example, sound from an aircraft on the runway or from vehicle traffic on the highway, which propagates horizontally initially above an acoustically hard concrete or asphalt surface and subsequently above a softer grass-covered surface. Several authors (refs. 20–23) have developed theoretical solutions to the problem of nearly horizontal sound propagation across an impedance discontinuity, and measurements both indoors and outdoors up to horizontal distances of a few meters have been made (ref. 24) for various types and distance ratios of hard and soft ground. In general there is good agreement between predictions and measurements, and in all cases the measured sound spectra are significantly different from what they would be for homogeneous ground, whether all hard or all soft. A typical example of a measured spectrum (ref. 24) is illustrated in figure 8 for a source 0.1 m high over asphalt and receiver 0.5 m high over grass where the propagation distances are 2 m and 6 m over the respective surfaces. Predicted spectra for a ground consisting of all asphalt or all grass are also shown, as well as the predictions of the spectra using the theories of references 21 to 23.

In the absence of specific calculations, which are time-consuming in many cases, one can postulate from the variety of measurement configurations shown in the figures of reference 24 that a good rule of thumb is to calculate the spectra by assuming first

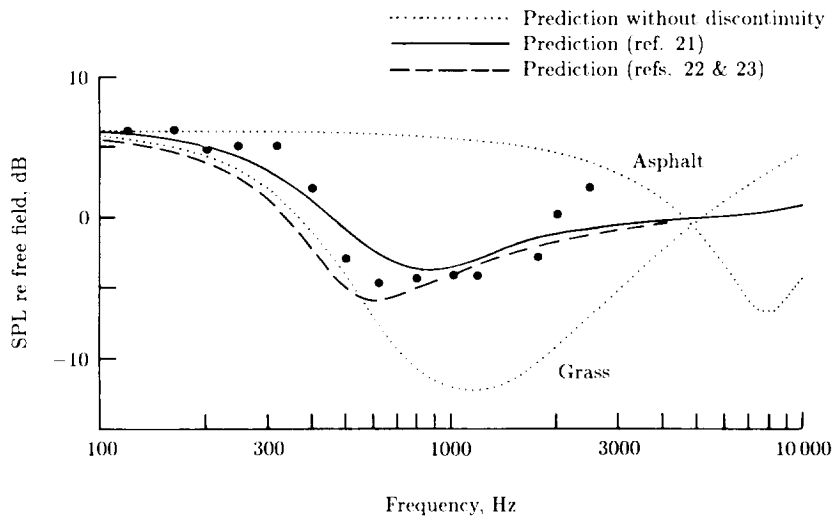

Figure 8. Measured changes in a sound field propagated across the impedance discontinuity between asphalt and grass. Source height 0.1 m above asphalt ($\sigma_e = 30 \times 10^6$ Pa-sec/m^{-2}) and receiver height 0.5 m above grass ($\sigma_e = 85 \times 10^3$ Pa-sec/m^{-2}); distances over surfaces were 2 m and 6 m, respectively. (From ref. 24.)

that the ground is all hard and second that it is all soft acoustically. A reasonably correct spectrum (within about 5 dB) can then be obtained by weighting the hard and soft spectra in proportion to the distances propagated over the hard and soft grounds.

Refraction by Vertical Gradients of Wind and Temperature

Under most weather conditions both the temperature and the wind vary with height above the ground. The velocity of sound relative to the ground is a function of temperature and wind velocity, and hence it also varies with height, causing the sound waves to propagate along curved paths. During the day solar radiation heats the earth surface resulting in warmer air near the ground. This condition, called a temperature lapse, is most pronounced on sunny days but can also exist under overcast skies. A temperature lapse is the common daytime condition during most of the year and ray paths curve upward.

After sunset there is often radiation cooling of the ground which produces cooler air near the surface. In summer under clear skies such temperature inversions begin to form about 2 hours after sunset, when they may extend to less than a meter above the ground; as the night progresses, they extend to increasing heights and can reach altitudes of the order of a hundred meters by sunrise. Throughout this period a temperature lapse exists above the top of the growing temperature inversion. Within the temperature inversion, the temperature increases with height and ray paths curve downward.

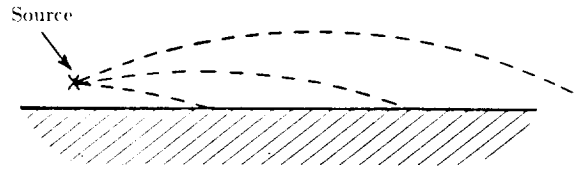

(a) Sound speed increasing with altitude.

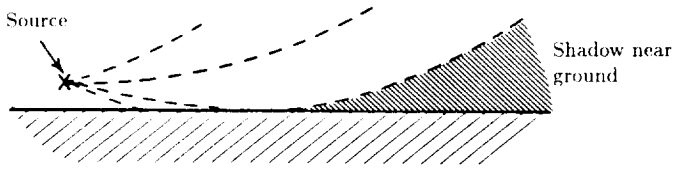

(b) Sound speed decreasing with altitude.

Figure 9. Schematic showing the bending of ray paths.

When there is wind, its speed decreases with decreasing height because of drag on the moving air at the ground. Therefore the speed of sound relative to the ground increases with height during downwind propagation and ray paths curve downward. For propagation upwind the sound speed decreases with height and ray paths curve upward. There is no refraction in the vertical direction produced by wind when the sound propagates directly crosswind. An illustration of the ray paths is shown in figure 9. In a temperature inversion or for propagation downward, the ray paths curve downward as in figure 9(a). Under specific conditions which depend on source and receiver heights, horizontal range, and the strength of the inversion, additional ray paths are possible that involve one or more reflections at the ground. In a temperature lapse or for propagation upwind, ray paths curve upward away from the ground as in figure 9(b). If the relation between sound speed and height is linear, there is a limiting ray that just grazes the ground and beyond which no direct sound energy can penetrate. This causes an acoustical shadow region. If, on the other hand, the sound speed profile is not linear, the limiting ray is replaced by a caustic because sound energy (rays) from various regions of the irradiated sound field can reach the same region along the shadow boundary. The effects of the temperature and wind profiles on the sound speed profile are additive. Rays curve upward or downward in the real atmosphere depending on the relative strength of the vertical gradients of temperature and wind speed. For example, an acoustic shadow can exist even downwind if the temperature lapse dominates the wind speed gradient to produce a sound speed that decreases with height. In what follows we shall distinguish between downward and upward refraction irrespective of which meteorological condition produces the effect.

Downward Refraction

The propagation of sound in a temperature inversion has been studied previously (ref. 25), but the principal results would be qualitatively similar for sound

propagation downwind. We shall therefore discuss here the more general case of a sound velocity profile that increases with height. The form of profile which is most convenient for physical interpretation and mathematical computation is one where the sound velocity increases linearly with height:

$$c = c_o(1 + \gamma h) \tag{13}$$

In equation (13), h is the height above the surface and γ is the coefficient of increase in velocity with height. We note that a linear variation with height is a good approximation for most cases although it is not necessarily achieved in practice. The sound rays between source and receiver are then circular arcs. When either the sound source or the receiver is above the ground, in addition to the direct ray there are reflected rays which also follow circular paths (fig. 10).

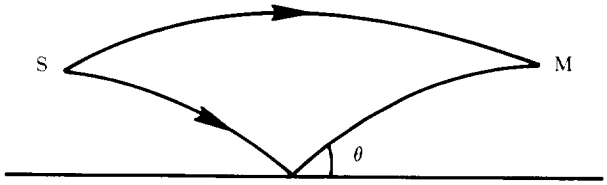

(a) At short or moderate source-to-receiver distances.

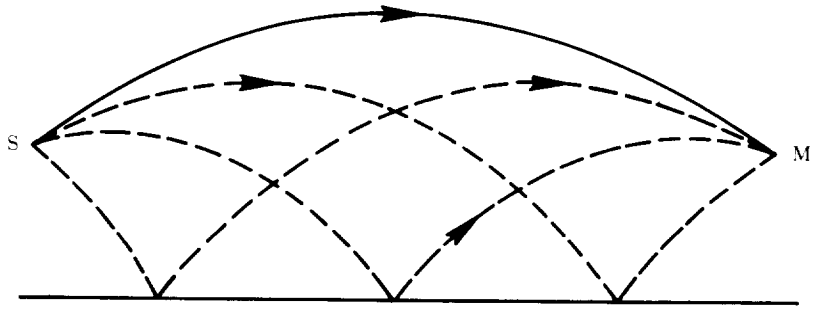

(b) At longer source-to-receiver distances.

Figure 10. Bending of ray paths in downward refraction.

If source and receiver are separated by moderate distances of the order of $d = 100$ m and are a few meters above the ground, there is only one reflected ray, providing that we also assume average atmospheric refraction. The direct and reflected ray paths are illustrated in figure 10(a). Note that the angle θ for the reflected ray is greater than for an unstratified atmosphere. The magnitude of the reflection coefficient therefore deviates further from -1 and the destructive interference between direct and reflected waves becomes less complete. The result is less attenuation for frequencies around 500 Hz. This is illustrated by the measurements (ref. 26) in figure 11. The curve labeled "0" represents sound levels measured in the absence of stratification or crosswind while the curve labeled "+5" represents results for downwind propagation. There is essentially no difference between those two curves below 400 Hz at 110 m or below 300 Hz at 615 m from

the source. At higher frequencies, however, the reduced attenuation for downwind propagation is evident.

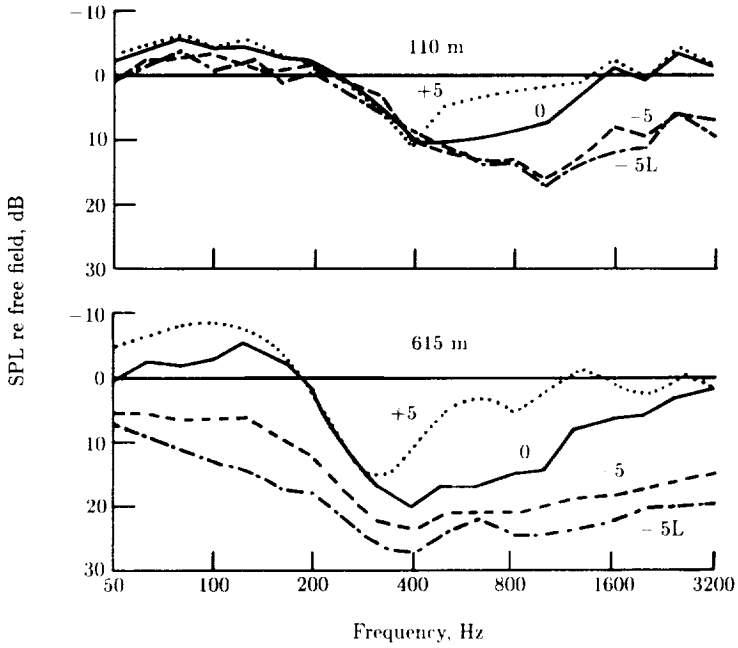

Figure 11. Sound pressure levels relative to free field in 1/3-octave bands of noise measured at 110 and 615 m from a jet engine (ref. 26). Numbers on curves indicate wind velocity, in m/sec, in the direction of propagation; curves marked "L" are for a temperature lapse. (From ref. 3.)

In general at longer distances d there are more than one reflected ray path (refs. 25 and 27). The existence of these additional ray paths is easily predicted (ref. 25) from elementary analytical geometry. Further, a particular ray may be reflected several times between source and receiver. When there is one reflection at the ground for any ray, there are three possible reflected ray paths. These are illustrated in figure 10(b) by the dashed curves. There is the ray reflected at the midpoint between source and receiver, assuming for the moment that the source and the receiver are at equal heights. The two other rays have a point of reflection displaced from this midpoint, one striking the surface relatively near the source and the other near the receiver. These additional paths further degrade the ground effect attenuation as shown in figure 11, at 615 m for frequencies above 400 Hz.

In the general case of finite source and receiver heights h_s and h_r, there are a total of four reflected ray paths for each number of reflections per ray greater than one. There is, however, an upper limit to the number of reflections at the surface, unless $h_s = h_r = 0$. It is not difficult to develop a simple criterion to determine the existence or absence of the higher order paths with multiple reflections. Let H_1 be the height of a ray path at its zenith (fig. 12). One can show for h_s and $h_r << d$, that

$$H_1 \approx \frac{\gamma d^2}{8} \tag{14}$$

where equality occurs when $h_s = h_r = 0$. Further, rays are realizable provided that

$$H_n \approx \frac{H_1}{n^2} \geq h_s \text{ and } h_r \tag{15}$$

Thus when n is sufficiently large that $H_n < h_s$ or h_r then the corresponding ray paths do not exist. To take specific examples, we assume that $h_s = h_r = 1.2$ m and $\gamma = 3 \times 10^{-5}$ m^{-1}, typical for a temperature inversion. Then, from equation (14), $H_1 = 0.04$ m for $d = 100$ m. Thus there is only one reflected ray path as shown in figure 10(a). Next, for $d = 800$ m, we find that $H_1 = 2.4$ m and $H_2 = 0.6$ m. This example corresponds to the illustration in figure 10(b). Finally at a much larger distance, for example, $d = 4$ km, equations (14) and (15) yield $H_1 \approx 60$ m and hence $H_7 \approx 1.2$ m and $H_8 \approx 0.9$ m. Thus, theoretically at least, there should be no ray paths having more than about seven reflections between source and receiver when both are 1.2 m above the surface.

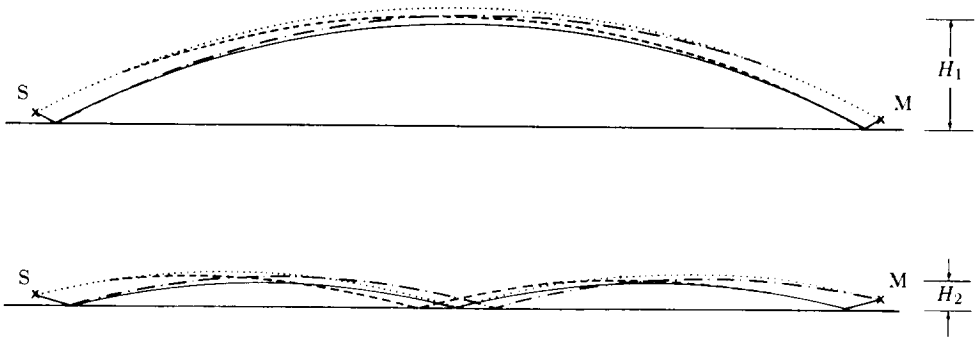

Figure 12. Schematic showing groups of ray paths in downward refraction that have approximately the same heights at zenith. (From ref. 25.)

At these larger distances, when the ultimate goal is to estimate the sound levels at a distant point as a result of sound traveling via the numerous ray paths, it is useful to group them differently from the number of reflections a ray suffered between source and receiver. A convenient grouping is according to the maximum height above the surface reached by the path as shown in figure 12. Thus the four rays having zenith heights of approximately H_1 have different numbers of surface reflections m; one has $m = 0$, two have $m = 1$, and one has $m = 2$. These rays follow almost the same path through the atmosphere and maintain partial coherence between themselves to a much greater extent than between other similar groups of ray paths. Under such conditions a method has been suggested (ref. 25) to estimate the sound levels at distant receivers. The interference between the direct ray from the source and the rays reflected at the surface are first calculated for the first grouping of individual rays in the bundle having zenith H_1. The amplitude and phase of the waves reflected near the source are calculated from the impedance of the surface, assuming that this is known, and added coherently to the direct ray, in effect assuming a composite source (see ref. 25 for the details of the calculations). Because the ground surface in the vicinity of the receiver can vary from one location to another, the sound rays reaching the receiver after a last reflection in the vicinity of the receiver should, on

average, be taken into account by adding their intensity to that of rays not suffering this reflection. If the reflection coefficient of the surface near the receiver is known to be unity, this implies adding 3 dB to the level given by the rays not reflected in this region. However a more typical magnitude for the reflection coefficient is less than unity and an average correction of 2 dB is suggested. The roles of sound source and receiver are reciprocal, so this discussion is valid also when the ground impedance near the receiver is known, but that near the source is not known or may vary from one source location to another. The sound energy traveling via the other groups of ray paths with zenith H_2, H_3, etc., experience different local turbulence (see the next section) and hence are expected to add incoherently to the energy via the primary group. The maximum correction to be added to the results calculated for the primary group is about 2.2 dB when there are an infinite number of possible paths (see ref. 25). In more realistic cases, when only a few of these paths exist, the correction to be added is about 0.5 dB. In most outdoor sound propagation problems this correction for multiple paths in downward refraction is therefore negligible.

The factors just discussed lead to the qualitative conclusion that downward refraction can nullify the reduction in sound pressure levels caused by ground effects. Sound levels therefore increase to the levels predicted by geometrical spreading and molecular absorption alone, but in general not above such levels. Increases above such levels are due to focusing caused by curved, that is, nonlinear, sound speed gradients and are inevitably accompanied by decreases caused by defocusing elsewhere in the sound field.

Upward Refraction

When the sound speed decreases with height, the sound rays are bent upwards, away from the ground. For realistic sound speed profiles, there is a limiting ray leaving the source which just grazes the ground. This limiting ray is shown in figure 13, and when the sound speed decreases linearly with height, the ray is an arc of a circle. Above this limiting ray the sound field is composed of direct and ground-reflected waves. Below the limiting ray there is an acoustical shadow region in which these waves theoretically do not exist; sound energy does however penetrate this shadow region due to other, diffractive propagation mechanisms.

It is perhaps useful to remind ourselves that rays do not represent any real physical entity. Rays are a convenient way of understanding various features of a sound field. For example, interference is a wave phenomenon that depends on phase differences between sound fields; rays provide a convenient set of geometrical lines from which path length differences, and hence phase differences, can be calculated. Similarly in figure 13 the limiting ray is a geometrical line whose trajectory can be calculated and which divides the sound field into two regions; the sound field is however continuous across the limiting ray, although it changes across a broad band of space near the limiting ray at a rate which depends on the wavelength of the sound and often on other geometrical factors—again, affirmation that what occurs in a sound field is governed by wave mechanisms.

Above the shadow region, the sound field can be described by the same arguments as before. A typical pair of direct and reflected waves is shown by the dotted curves in figure 13 to the point M_1. There is always only one ground-reflected wave and the incidence angle θ is smaller than for the unstratified atmosphere. The magnitude

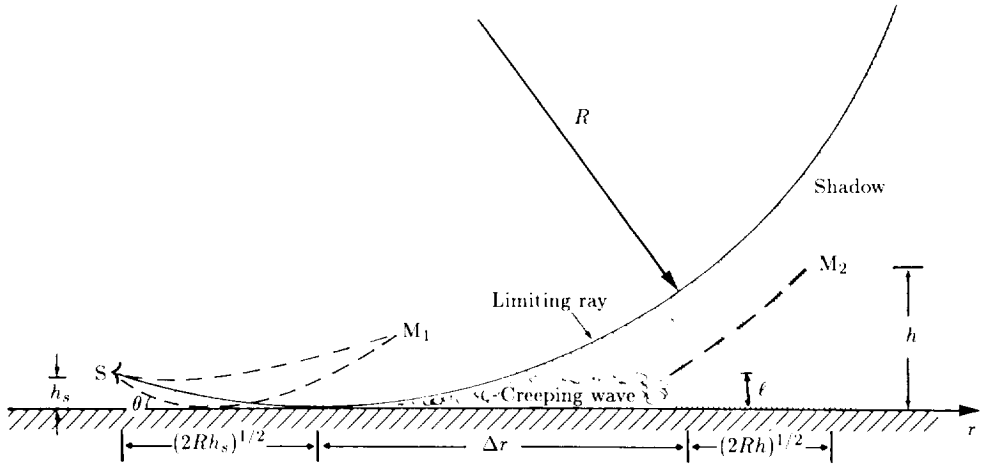

Figure 13. Schematic illustrating the main features of upward refraction. (From ref. 31.)

the reflection coefficient is now closer to −1 and the destructive interference between direct and reflected waves is enhanced. This increases the attenuation for frequencies above about 500 Hz (see the curves in fig. 11 at 110 m, labeled "−5" for upwind propagation and "−5L" for lapse conditions). These results were probably measured just beyond the limiting ray into the fringe of the shadow; however the results still show the effect described above. Theory to account for the changing incidence angle due to the curved ray path has been described in reference 27, where calculated curves predicted well the changes in the spectra of figure 11 at high frequencies.

At 615 m from the source the results labeled "−5" and "−5L" in figure 11 were measured farther into the shadow region (M_2 in fig. 13) and the description of these results requires a very different analysis. A number of numerical methods are available to compute accurate quantitative results (refs. 28 and 29). These reconstruct the sound field allowing for the effects of diffraction, changes in sound velocity with height, or other relevant factors. However to provide a better understanding of the features involved, we shall describe the process in an alternative and more intuitive way. The sound levels, in the absence of turbulence, can be determined from diffraction theory (ref. 30), which suggests that the energy received at M_2 initially leaves the source and travels along the limiting ray to the ground. Then it propagates in the air along the surface in a creeping wave. At an appropriate distance, the energy is then shed from the creeping wave and travels to M_2 along the ordinary geometrical acoustics ray shown by the dashed curve in figure 13. An example of an acoustical shadow governed by this mechanism is shown in figure 14. The points are measurements made above an asphalt surface at a distance of 200 m from a point source (ref. 31), at locations well within the shadow region. Predictions obtained from creeping-wave theory, the solid curves, are in reasonable agreement with the measured values except at the two highest frequencies close to the ground and upwind, that is, where the sound pressure levels are lowest. This discrepancy

is probably due to yet another mechanism, scattering by turbulence, whereby sound energy is redistributed between various regions of otherwise coherently determined sound fields.

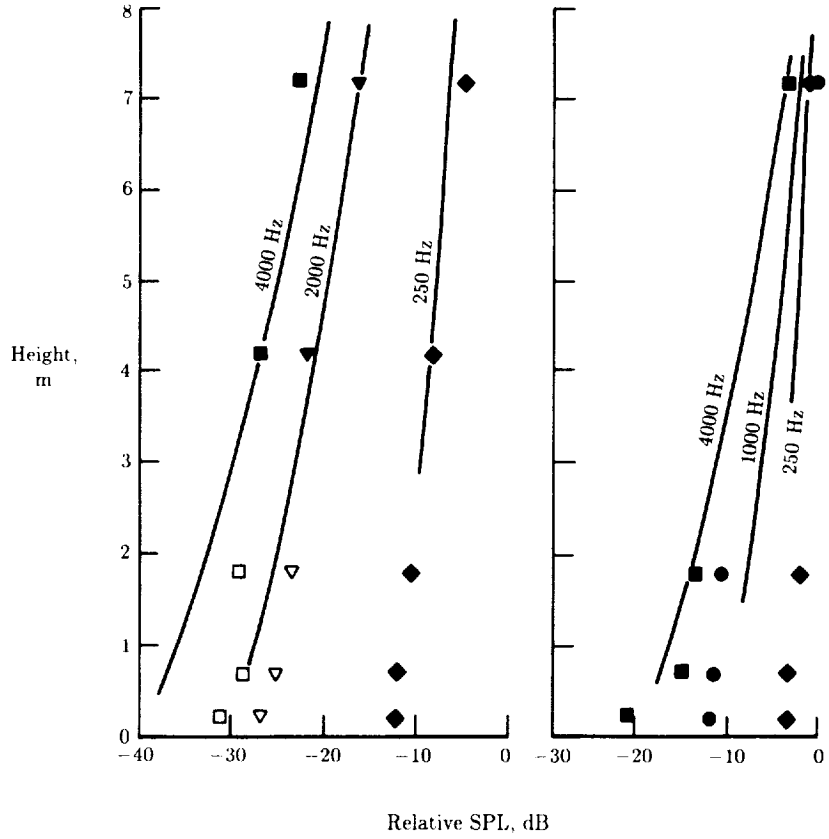

(a) Upwind. *(b) Downwind.*

Figure 14. Comparison of predicted and measured sound pressure levels within shadow region at a distance of 200 m from the source over an asphalt surface. Sound pressure levels marked by open symbols may be perturbed by turbulence. (From ref. 31.)

Atmospheric Turbulence

The atmosphere is an unsteady medium (ref. 32) with random variations in temperature, wind velocity, pressure, and density. In practice only the temperature and wind velocity variations significantly affect acoustic waves over a short time period. During the daytime these inhomogeneities are normally much larger than is generally appreciated. Shown in figure 15 is a typical record of the temperature measured 1 m above a flat ground surface on a sunny day. The measurement was made with a fast response (< 1 msec) thermometer. Fluctuations in temperature of

5°C which last several seconds are common and 10°C fluctuations not uncommon. The wind velocity fluctuates in a similar manner and has a standard deviation about its mean value that is commonly one-third of the average value. When waves propagate through the atmosphere, these random fluctuations scatter the sound energy. The total field is then the sum, in amplitude and phase, of these scattered waves and the direct line-of-sight wave, resulting in random fluctuations in amplitude and phase. The acoustical fluctuations are in some respects analogous to more familiar optical phenomena such as the twinkling of light from a star.

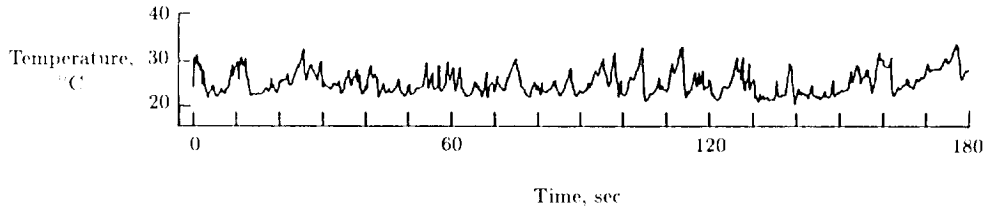

Figure 15. Typical recording of the temperature measured about 1 m above the ground on a sunny summer day. The response time of the thermometer was less than 1 msec.

Large eddies are formed in the atmosphere as energy is injected into the turbulence as a result of instabilities in the thermal and viscous boundary layers near the ground. For example, we have seen in the section on refraction that the average horizontal wind velocity varies as a function of height, being essentially zero at the ground surface, and this variation creates turbulence of a size approximately equal to the height. This is illustrated very clearly in reference 33. The size at which the energy enters into the turbulence is called the outer scale of turbulence and is designated by L_o. The eddies of sizes greater than L_o are generally anisotropic. The spectrum in this range, called the input range, depends on how the turbulence is created in the particular circumstances, and thus there is no general formula describing the turbulence characteristics in this range.

In the range of the spectrum where the eddy size is smaller than L_o, the kinetic energy of the turbulence is very much greater than the amount of kinetic energy that can be dissipated due to viscosity in the time required for a large eddy to break down into smaller eddies. Since the dissipation is negligible, almost all the kinetic energy can be transferred to eddies of smaller size. Thus, the energy transfer can be visualized as a process of eddy fragmentation where large-scale eddies cascade into eddies of ever-decreasing size. The characteristics of the initial conditions disappear, the fluid motion is almost completely random and irregular, and its features can be described in statistical terms. This part of the turbulence spectrum is called the inertial or Kolmogorov range.

However, as the eddy size becomes smaller, the fraction of available kinetic energy being dissipated by viscosity increases. Eventually the smallest size ℓ_o of the eddies is reached where their kinetic energy is of the same order as the kinetic energy being dissipated. At this size ℓ_o, virtually all the energy is dissipated into heat and almost no energy is left for eddies of size smaller than ℓ_o. This size ℓ_o is called the inner scale of turbulence and is typically of the order of 1 mm. The spectrum range of eddy size smaller than ℓ_o is called the viscous range.

The three characteristic ranges of the spectral density of the turbulent atmosphere are illustrated in figure 16. The points are an example of a measured spectrum of wind velocity fluctuations. Essentially, the points represent the fast Fourier transform (FFT) of the time-varying signal recorded by the anemometer. The measurements were made about 1 m above the ground and, as expected, the outer scale is about 1 m.

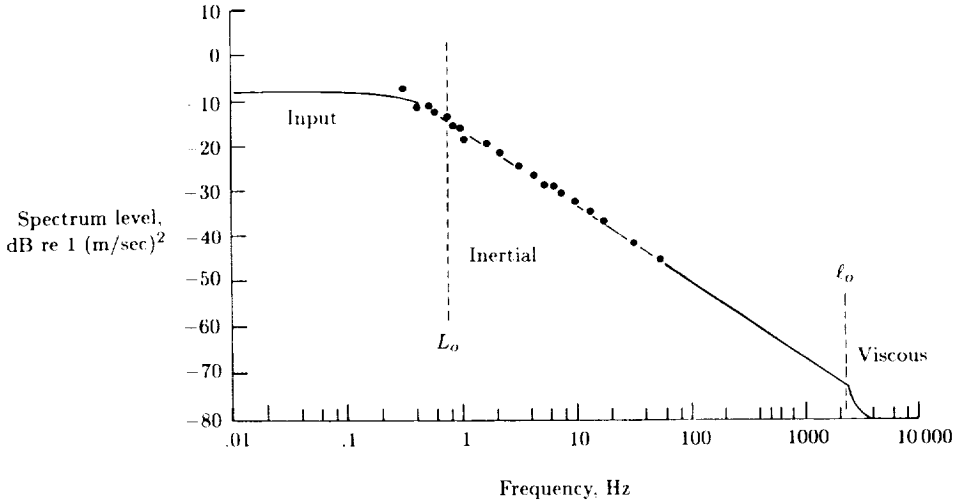

Figure 16. The three ranges of the atmospheric turbulence spectrum. The points are the result of an FFT analysis of a wind velocity recording.

For horizontal sound propagation near the ground in the range of frequencies from a few hundred to a few thousand hertz and distances of hundreds of meters, the propagation is most influenced by eddies having sizes greater than 1 m and hence in the input region of the turbulence spectrum. As explained above, there is no general formula describing the turbulence in this range. Measurements and some simple theory, although still tentative, are beginning to provide information on the mechanism governing the propagation through turbulence in this range (refs. 31 and 34). On the other hand, for air-to-ground propagation from an elevated source, the outer scale is much greater than 1 m and the propagation is most influenced by eddies in the inertial range of turbulence. Our understanding of the mechanism in this case is much better, mainly because of the large body of knowledge accumulated through work on atmospheric sounders (ref. 35).

Regardless of whether the significant turbulence is larger or smaller than the outer scale, the scattering of sound by turbulence produces fluctuations in the phase and amplitude of the received signal. The magnitude of the fluctuations increases with increasing distance of propagation, sound frequency, and strength of turbulence. Shown in figure 17 are measured phase (open points) and amplitude (solid points) fluctuations plotted as a function of the calculated fluctuations (ref. 34). The measured fluctuations are for a variety of frequencies, distances of propagation, and strengths of turbulence. The calculated values are obtained from simultaneous meteorological measurements. The graph shows that the phase fluctuations increase without bound, as predicted, for increasing values of the variables. The amplitude

fluctuations on the other hand, in addition to being systematically lower than the phase fluctuations, clearly show saturation.

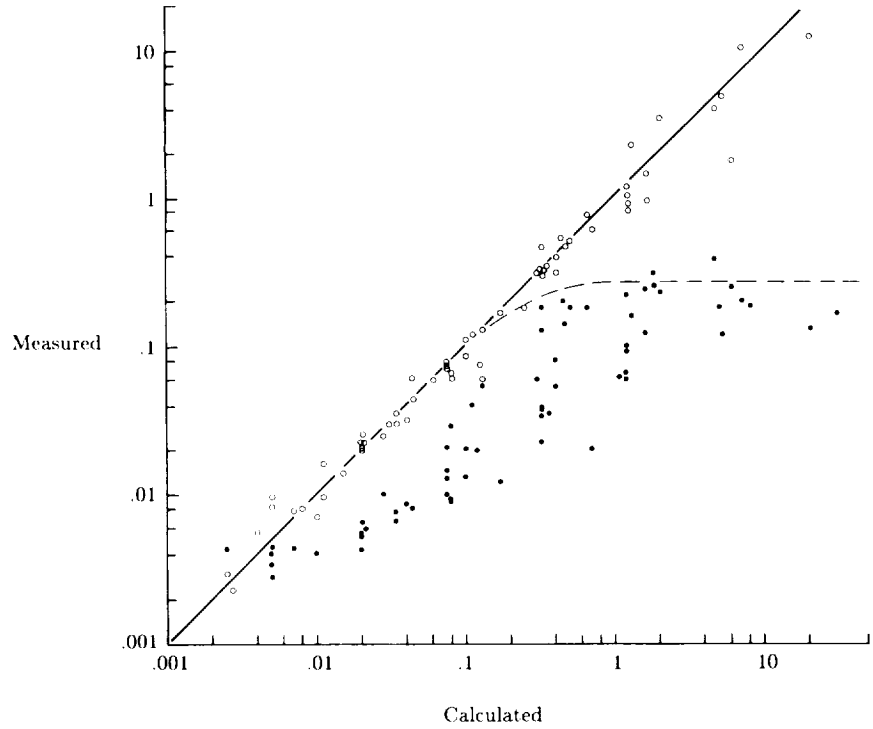

Figure 17. Measured amplitude (solid points) and phase (open points) fluctuations as a function of the corresponding calculated values. (From ref. 34.)

An effect of atmospheric turbulence, which is immediately suggested by the results shown in figure 17, is the nuisance of coping with fluctuating levels during noise measurements from relatively distant sources such as aircraft. However the saturation of the amplitude fluctuations shown in figure 17 minimizes this problem. The fluctuations in sound pressure level initially increase with increasing distance, but quickly reach a limiting value. For example when the noise from aircraft propagates under clearly line of sight conditions over distances of a few kilometers, the measured sound pressure levels fluctuate about their mean value with a standard deviation of no more than 6 dB. This is in agreement with the results of figure 17.

An effect of atmospheric turbulence which has traditionally been considered important is the direct attenuation of sound by turbulence. If the sound is in a highly directed beam, the turbulence attenuates the beam by scattering energy out of it (ref. 36). However for a spherically expanding wave this attenuation is negligible, because the scattering from turbulence is elastic and mostly in the forward direction through a small scattering angle. Therefore, in a simpleminded way, the energy scattered out from the line of sight is replaced by energy scattered back to the receiver from adjacent regions. This implies that the energy level of the root-mean-square sound pressure in an unsteady medium is the same as the level would be in the absence of turbulence. The only mechanism by which turbulence could

provide attenuation in a spherical wave field is backscattering (ref. 37). However it seems that the attenuation provided by backscattering is much smaller than the attenuation due to molecular absorption. The attenuation of sound due to scattering from a moderately directional source must lie between the two extremes of a finite-width beam and a spherical field, but has never been evaluated thoroughly. It is generally believed (ref. 3) to be negligible for most applications.

Other acoustical phenomena are most strongly and directly affected by atmospheric turbulence. For example the interference of direct and ground-reflected waves depends critically on the exact phase relationship that exists between them. The random fluctuations in phase shown in figure 17 bring into question the use of coherent acoustical theory to describe this phenomenon, as was done earlier. The points in figure 18 are excess attenuation measurements from reference 26 of jet noise propagating across a grass-covered field for various distances. (Excess attenuation is that which is over and above attenuation due to normal spreading and atmospheric absorption.) The dashed curve is calculated using the coherent acoustical theory described earlier. At frequencies below about 300 Hz, this theory adequately describes the measured values. However, above 300 Hz, the coherent theory begins to consistently overpredict the depth of the ground shadow at a distance of 100 m. The discrepancy between the measured points and the solid curve reaches about 10 dB at a distance of 1 km. The solid curves were calculated (ref. 38) by treating the atmosphere as a turbulent medium and assuming a normal distribution of phase velocities of sound having a standard deviation of about 2 parts per 1000 and some partial coherence between the direct and the reflected path. Theory (refs. 38–40) shows that the partial coherence between the two paths is very sensitive to the ratio of path separation and coherence length of the medium. A coherence length of about 1 m, typical of values measured close to the ground, was used to calculate the curves in figure 18. To assume partial, rather than complete, coherence between the interfering waves is the only simple way to obtain reasonable agreement with measurements at all frequencies and distances. Alternatives such as using a different value of ground impedance could have secured agreement at some frequencies only at the expense of worse agreement elsewhere in the spectrum or at other distances.

Another example of the degradation of an acoustical shadow region was discussed in the previous section. The measurements shown by the open symbols in figure 14 suggest that, in addition to the energy that is diffracted into the shadow region, the sound scattered by turbulence is contributing to the total level. Although there is as yet no direct quantitative calculation to support this hypothesis, it is consistent with model experiments (ref. 41) using thin barriers.

In summary, atmospheric turbulence was evoked in the past to account for decreased sound levels that did not appear to have any other explanation. However this was before the role played by many of the relevant wave propagation mechanisms had been appreciated. Now work is showing why, and to what extent, turbulence enhances the sound levels in the various types of shadow regions.

Discussion

Up to now we have discussed the consequences of the finite impedance of the ground on sound propagation outdoors in an ideal atmosphere. The discussion was then extended to a stratified atmosphere with curved ray paths, but in the absence of

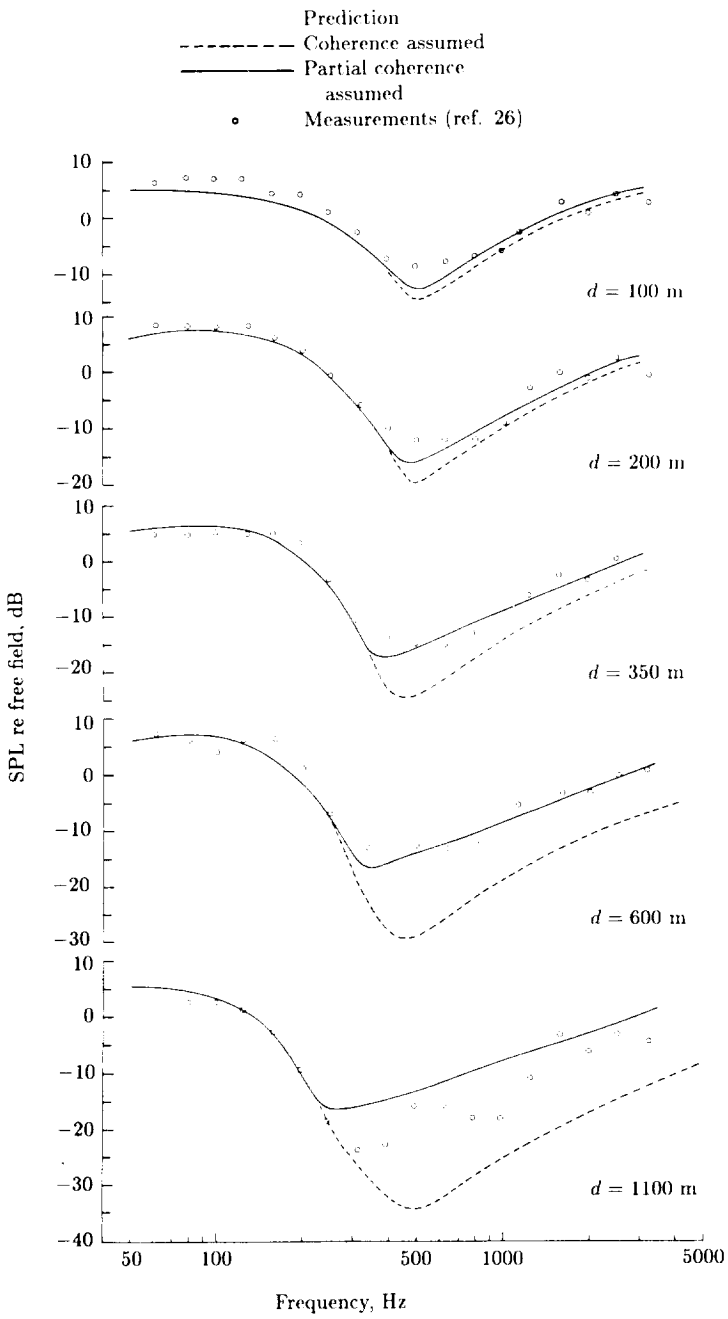

Figure 18. Comparison of measured sound levels (ref. 26) with values predicted from theory for jet noise propagating over a grass-covered field. (From ref. 38.)

turbulence, and subsequently to include the effects of the turbulent atmosphere, but for straight line propagation. It is possible, at least theoretically, to assume straight line propagation in a turbulent atmosphere. This could happen for propagation downwind on a sunny day when, fortuitously, the wind velocity gradient equals the temperature gradient in magnitude but differs in sign, to produce a zero sound speed gradient. In practice, situations do occur where the sound speed gradient is negligibly small and there is a body of theory (refs. 33 and 38–40) that accounts for partial coherence due to turbulence and which shows reasonable agreement with measurements (refs. 33 and 38).

However the idealization of a nonturbulent but stratified atmosphere may be rarely achieved in practice. The presence of strong wind and temperature gradients is usually accompanied by atmospheric turbulence. An exception could be a temperature inversion in the absence of wind. Fortunately it is not difficult to extend an existing model (ref. 27) to allow for partial coherence between the curved ray paths.

An example of such a calculation is shown in figure 19. The curves are calculated relative sound pressure levels as a function of distance for two frequencies and three atmospheric conditions. The solid curves assume propagation above grass-covered ground in a zero sound speed gradient but in the presence of atmospheric turbulence which could correspond to a Turner class (ref. 33) of 1. This calculation has been previously presented for one frequency in reference 31. At 125 Hz or any other low frequency the result is indistinguishable from theory that neglects atmospheric turbulence. However at 1.2 kHz the solid curve differs significantly from the prediction of coherent theory. This latter theory begins to predict lower sound pressure levels at a distance of about 50 m to attain −25 dB at 1 km, for a discrepancy of 15 dB between coherent theory and the solid curve.

The short-dashed curves are calculated for a slightly less turbulent atmosphere but, in addition, for a positive sound speed gradient (downward refraction). Beyond 400 m, ray theory predicts the existence of additional ray paths (see eq. (15)). At 125 Hz the results differ little from coherent theory. On the other hand at 1.2 kHz, the increased incidence angle, the additional ray paths beyond 400 m, and the loss of coherence all contribute to almost eradicating the attenuation produced by the finite impedance of the ground (at the larger distances where there are many ray paths, a simpler calculation was performed (ref. 25)).

The long-dashed curves were calculated for a slightly more turbulent atmosphere than the short-dashed curves but now for a negative sound speed gradient (upward refraction). The shadow boundary expected from ray theory occurs at 400 m. Therefore, beyond 400 m the curve is calculated using diffraction theory (ref. 31). At 125 Hz the long-dashed curve differs from the solid curve only beyond 400 m, that is, in the shadow region that exists in this case. At 1.2 kHz the long-dashed curve differs negligibly from the result that would be obtained using coherent theory up to about 400 m. This is because the reduced incidence angle of the reflected wave produces lower sound pressure levels which are then enhanced because of partial coherence between direct and reflected waves. For this particular calculation the two effects almost cancel. Beyond 400 m the levels are determined by diffraction theory up to some relative sound pressure levels shown by the shaded area. The body of available experimental data (refs. 3, 26, and 31) shows that, in practice, lower sound pressure levels are not achieved in a turbulent atmosphere. There is no

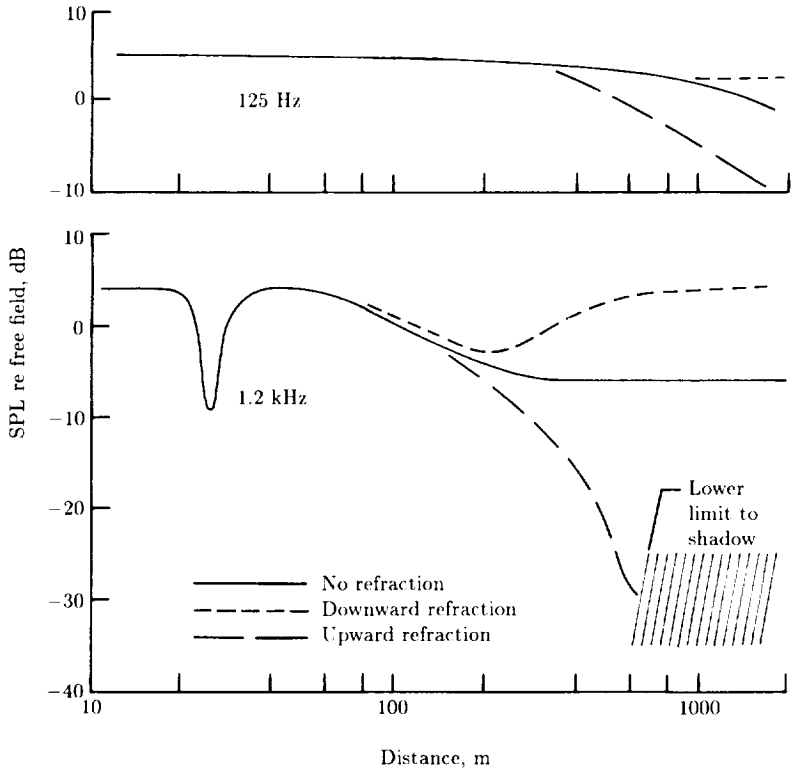

Figure 19. Comparison of predicted sound pressure levels as a function of distance for two frequencies and three atmospheric conditions. Propagation over grass in presence of atmospheric turbulence.

rigorous theory to substantiate this at present. However there is some theory (ref. 41) and experimental evidence (ref. 31) to support the explanation that scattering by turbulence is responsible for these limiting sound pressure levels.

The features shown for the 1.2-kHz calculation are also found for frequencies between 200 and 2000 Hz, but differ in detail. The results also differ in detail for different atmospheric conditions, but the main tendencies remain. The curves are examples of typical behavior justified on physical arguments and are consistent with the behavior of experimental data (see fig. 13 of ref. 31 and the data in ref. 26).

In summary, because of variations in atmospheric conditions, it is not possible to produce a unique prediction of sound pressure levels, especially for distances greater than about 50 to 100 m. The levels will not exceed those given by inverse square law and molecular absorption (unless there are sufficient multiple downward refractive paths in which case the level may be enhanced by 1 to 2 dB) but can be, and usually are, lower because of a combination of other mechanisms; the levels are rarely lower by more than −25 to −35 dB because of the turbulent atmosphere.

Diffraction

The processes of diffraction arise from the mutual interaction of neighboring elements of a wave field. They occur when the amplitude and phase of the sound

field vary spatially in ways that are incompatible with the sound wavelength at any given frequency. Far from any boundaries a sound field propagates in a relatively simple way, and one can exploit this simplicity by describing the propagation in terms of ray paths. However if a large solid body blocks the sound field, the ray theory of sound propagation predicts a shadow region behind the body with sharply defined boundaries, so in principle, on one side of the boundary there is a sound field with well-defined phase and amplitude and close by on the other side of the boundary there is essentially silence. This does not happen in practice; as the waves propagate, sound "leaks" across this sharp boundary in ways governed by the laws of wave motion and the boundary becomes less sharp. Diffraction effects are most clearly evident in the vicinity of solid boundaries, or along geometrical ray boundaries such as the limiting ray shown in figure 13.

Acoustic diffraction occurs in conjunction with a wide range of solid bodies: some such as thin solid barriers are erected alongside highways or are carefully located to shield residential communities from ground operations of aircraft; others such as buildings are often built for other purposes but fortuitously provide some beneficial shielding; yet others like undulating ground or low hills occur naturally and provide shielding at much larger distances and bring forth other manifestations of diffraction such as the creeping waves referred to earlier.

Most of the development of diffraction theory for sound waves has been adapted from optical diffraction theory (refs. 42–44). It has been applied mainly to understand and accurately predict the performance of thin barriers, including the practical situations of barriers standing on ground of finite impedance, where effects due to ground reflections and interference interact with diffraction of sound over the top of the barrier (ref. 45). Other developments have been to describe the shielding behavior of thick barriers (refs. 46 and 47), such as buildings or earth berms.

The simplest and most widely used procedure for determining the reduction of sound pressure level due to diffraction around the edge of a barrier is described in reference 48. One must first calculate the Fresnel number, which is simply the minimum increase in distance that the sound must travel around the edge of the barrier to go from source to receiver (fig. 20), divided by a half-wavelength $\lambda/2$ at the frequency of interest. The Fresnel number N is

$$N = \frac{2}{\lambda}(d_1 + d_2 - d_3) \tag{16}$$

The reduction in sound pressure level is then given as a function of Fresnel number by the curve in figure 21. This curve is obtained from diffraction theory assuming a thin knife-edge barrier and no ground and then empirically allows for the presence of the ground by reducing the loss of sound level by about 2 dB. This prediction curve is not exact because the empirical correction does not account for the frequency dependence (here, the Fresnel number dependence) of the ground-reflection interference in a specific configuration of source, barrier, and receiver heights and distances apart. The curve is correct to about ±5 dB in most cases and is the mean curve through the interference spectrum that would be measured, and can be predicted, in any specific circumstances.

In practice the reduction in sound pressure level behind a barrier rarely exceeds about 15 to 25 dB, except in extreme configurations when the diffraction angle, θ

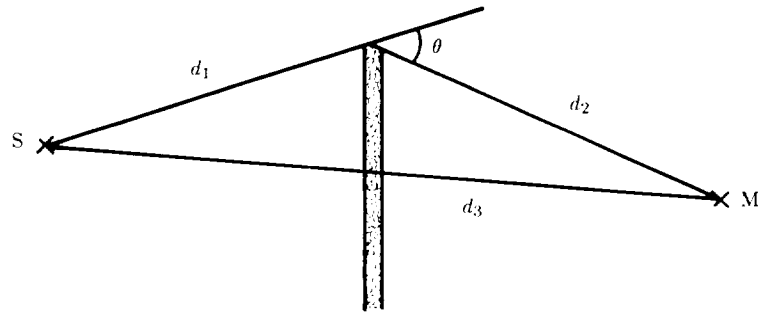

Figure 20. Schematic defining the necessary parameters for diffraction around a thin barrier.

in figure 20, is very large. More commonly the performance of a barrier is limited to these values by the effects of the turbulent atmosphere (ref. 41). As discussed previously, scattering by turbulence provides an additional mechanism by which sound energy can penetrate the shadow behind the barrier, thus resulting in an upper limit to the reduction in sound pressure level. If the barrier is not continuous, such as a row of detached houses, other empirical values are sometimes used. For example, when the gaps between houses are 30 to 50 percent of the whole, a drop of 2 to 3 dB is sometimes assumed for one row of houses, about 4 to 6 dB for two or more rows. These are obviously average values and are greater directly behind a house and much less in line with the break in the barrier.

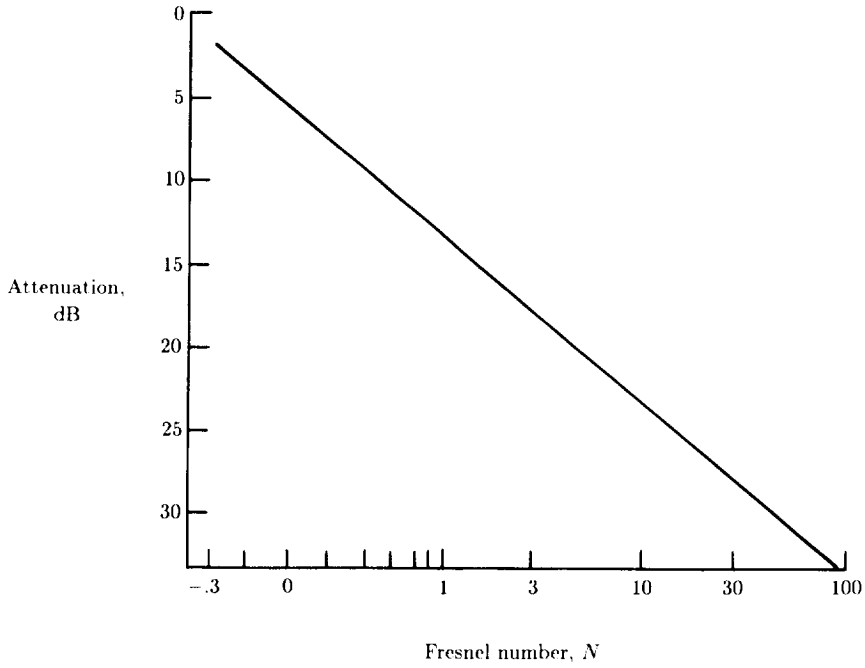

Figure 21. Reduction in sound pressure level relative to the free field without a barrier as a function of Fresnel number N. (Curve from ref. 48.)

When barriers are used specifically to reduce sound, it is good practice to locate them, when possible, as closely as possible to either the source or the receiver. A barrier of given height then results in a large value of the diffraction angle θ and a greater path lengthening $(d_1 + d_2 - d_3)$. This provides a larger insertion loss and also more protection against degradation of this insertion loss by refractive effects that, under appropriate meteorological conditions, can cause the direct sound field to curve around the edge of the barrier. It is difficult to be precise because the variables are so many, but refractive effects can often bend sound fields through a few degrees in a distance of 100 m: this suggests that the diffraction angle θ must be at least 5° for a sound barrier to provide some amount of diffractive shielding under most meteorological conditions.

At distances between source and receiver greater than a few hundred meters, it is difficult to provide man-made barriers large enough to provide any noticeable reduction in sound pressure levels. Naturally occurring topographical features such as hills can often function as barriers, blocking the line of sight between source and receiver. There has been very little systematic study of the acoustical effects of terrain shape and type at long ranges, partly because of the wide range of possible forms and the difficulties of understanding the general principles that could then be applied to other terrains and partly because dominant meteorological effects would often cast considerable uncertainty on any terrain-related results. The processes of diffraction can however assist in understanding one very simple form of ground shape, namely a spherical or cylindrical surface that curves downward. There is a close analogy between a ground surface that curves downward in conjunction with sound rays that travel in straight lines and a ground surface that is flat while sound rays curve upward because of a temperature lapse or upwind propagation. The analogy is shown in figure 22, where the reader will recognize that figure 22(b) has extracted the relevant features from figure 13 that was earlier used to describe the behavior of sound fields in upward refraction due to meteorological gradients. Measurements and relevant theory (refs. 49–52) on grass and asphalt surfaces outdoors and artificial surfaces indoors having shapes corresponding to figure 22(a) are the subject of current work. Typical results (ref. 49) for propagation around a grass-covered cylindrical mound having a radius of curvature of 25 m are shown in figure 23 for two source-to-receiver distances and three receiver heights all within the shadow region.

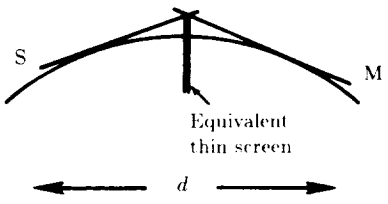

Sketch A

The short dash curves in figure 23 represent the prediction of simple diffraction theory when the curved surface is replaced by an equivalent thin barrier, with the height of the equivalent barrier being determined by line-of-sight geometry as shown in sketch A on the left. This prediction is reasonably good at low frequencies, here below about 500 Hz, but at higher frequencies it underestimates the measured shadow by as much as 20 dB. The short-long dashed line in figure 23 is the prediction for creeping-wave diffraction mechanisms assuming a surface of infinite impedance, and the lower solid line was calculated (ref. 51) assuming a grass-covered surface of finite acoustic impedance. The trend of the measured values is clear for both receiver heights and is as expected from the ground impedance values shown in figure 5—at the lower frequencies the ground impedance is higher and can be idealized as a rigid boundary;

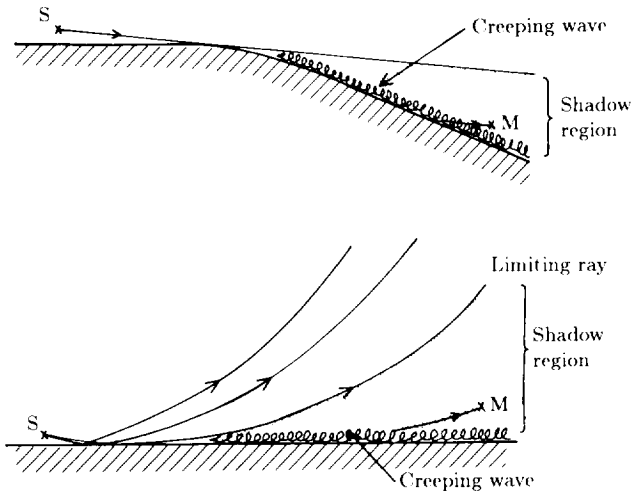

Figure 22. Analogy between sound propagation in a homogeneous, isotropic atmosphere over downwardly curving ground and sound propagation in an upwardly refractive atmosphere, above a flat ground.

as frequency increases there is a smooth transition to the predictions assuming a low acoustic impedance. The discrepancy between the measured points and the lower solid line at $d = 11$ m and $h_r = 0.25$ m is attributed to atmospheric turbulence (ref. 41).

Thus we see that diffractive mechanisms play an important part in the propagation of sound fields. These mechanisms are responsible for determining the sound pressure levels in acoustical shadow regions, whether these shadow regions are produced by solid obstacles at short or long ranges or by refractive processes causing the upward bending of sound rays.

Large-Amplitude Waves, Pulses, and Sonic Booms

The discussion of sound propagation mechanisms so far in this chapter, as in most of the acoustical literature, has assumed that sound waves propagate according to linear laws in a linear medium. It has been assumed, for example, that the speed of sound is a constant determined only by the properties of the air, principally its temperature; that the frequency and wavelength of a given sound do not change during propagation or as the sound is subjected to any of the mechanisms described so far; and that the amplitude of the sound, and its spectral content, change during these processes by the same fraction (or its sound pressure level by the same number of decibels) regardless of whether the sound initially has a high or a low sound pressure level. For many acoustical problems the assumptions of linearity, superposition of waves, and the approximations of small-amplitude acoustics are perfectly adequate.

When a sound source is sufficiently intense or when the sound field remains at a high enough level for a sufficient distance of propagation, then nonlinearity of many of the wave propagation processes becomes important, gives rise to many further phenomena, and can significantly affect the sound received by a distant observer.

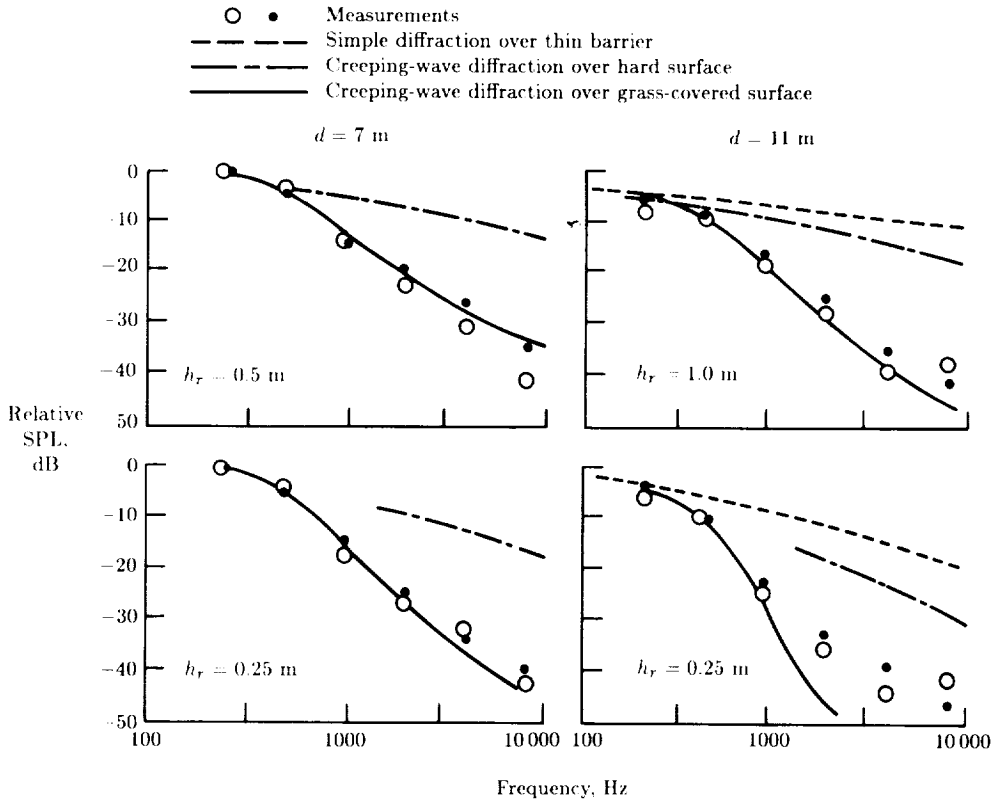

Figure 23. Sound pressure levels over a grass-covered curved ground with radius of curvature of 25 m. Source on the ground.

Here we shall focus attention on one small group of nonlinear phenomena that are all related to the fact that the propagation speed of any part of the waveform depends on its own particular particle velocity. The result is that waveforms change shape during propagation, their spectral content changes, shock waves may develop, and there is increased absorption.

Waveform Distortion

As a sound wave propagates through air, the instantaneous pressure, particle velocity, temperature, and density at any point in the waveform all vary simultaneously and are closely related. In that part of the waveform where the pressure increases, the temperature and density also increase, and the longitudinal particle velocity due to the wave is in the direction in which the wave energy is propagating. (Conversely when the pressure, temperature, and density simultaneously decrease, the particle velocity is in the opposite direction to that in which the energy is being propagated.) The zero crossings of the sound waveform travel with the "small-amplitude" speed of sound, c_o = 331.2 m/sec at 0°C, which is the speed of sound described earlier. However other parts of the waveform, which we intuitively and most commonly think of as a pressure waveform, each travel relative to the local part of the propagation medium (refs. 53 and 54). There are two distinct effects on the speed with which

individual elements of the waveform propagate. Consider an element of the wave having an instantaneous positive pressure: first the temperature is momentarily increased due to the sound wave and so the local speed of sound is increased to a value given by

$$c = c_o + \frac{\gamma - 1}{2} u \tag{17}$$

where γ is the ratio of specific heats of air ($\gamma \approx 1.4$) and u is the local particle velocity. Second the waveform travels relative to the local medium which in this region of positive pressure is traveling in the forward direction, also with the particle velocity u. The net result is that this part of the waveform travels with a velocity

$$c = c_o + \frac{\gamma - 1}{2} u + u = c_o + \frac{\gamma + 1}{2} u \tag{18}$$

Equation (18) is a general result that applies to all elements of a continuous waveform; in particular when the acoustic pressure is negative, the particle velocity is in the opposite direction and the negative half-cycle of the waveform travels in the direction of propagation more slowly than the zero crossings. Furthermore the excess velocity relative to c_o for the zero crossings is proportional to the particle velocity u (or proportional to the acoustic pressure p through the impedance relation $p/u = \rho c$ where ρ is density). Thus the positive peak of a waveform travels fastest and "catches up" to the zero crossing ahead of it, while at the same time increasing its separation from the zero crossing that follows it. The opposite process occurs for the negative peak of the waveform. The net result of these differences in propagation speed is that the waveform changes shape during propagation as illustrated in figure 24.

Figure 24 represents the pressure vs. time waveform that would be detected at successively increasing distances of propagation. The wave is assumed to be an infinitely long series of initially sinusoidal waveforms, one cycle of which is shown in figure 24(a); it propagates from right to left, and retarded time is used to reduce the corresponding zero crossings to $t = 0$ in each case. In those parts of the waveform where $\partial p/\partial t$ is positive, this gradient increases with distance of propagation; where negative, this gradient becomes less steep. At some distance the rate of change in pressure may become infinitely steep (in reality, it is finite but can take place over a distance of the order of a mean free path of the gas molecules if the pressure difference is sufficiently great) and this denotes the formation of a shock wave. In an initially symmetrical sinusoidal waveform this discontinuity occurs at those zero crossings where pressure is increasing (fig. 24(c)). As the waveform continues to propagate, the shock wave extends over a bigger change in pressure as regions of lesser pressure immediately ahead are overtaken by it, and higher pressure regions behind the shock catch up to it. A shock wave represents an abrupt change in acoustic pressure and a discontinuity in particle velocity, but once formed it travels with a velocity that is the mean of that associated with the pressures and velocities immediately ahead of and behind it. Hence, for an initially symmetrical sinusoidal waveform, the resulting shock waves remain symmetrical and travel with the small-amplitude speed of sound with the result that each cycle of the wave train remains of constant wavelength and fundamental frequency.

Once a shock wave is formed, continued use of equation (18) leads to the situation shown by the dotted waveform in figure 24(d), in which three different pressures

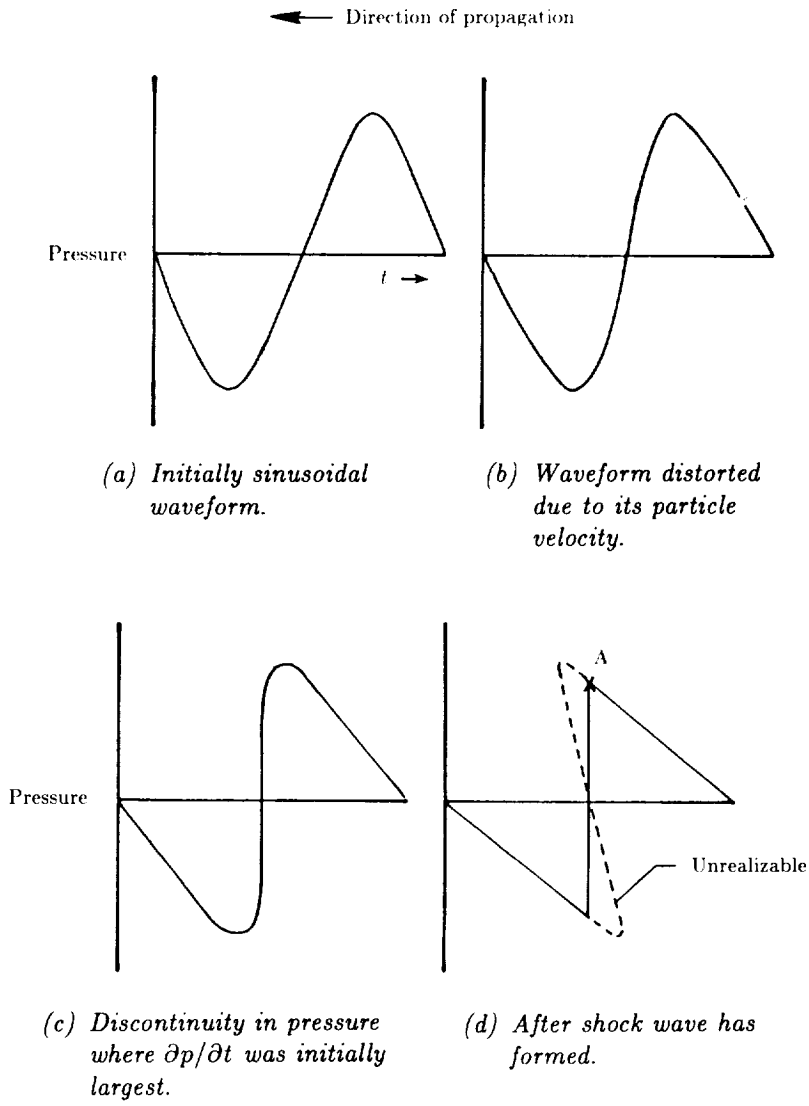

(a) Initially sinusoidal waveform.

(b) Waveform distorted due to its particle velocity.

(c) Discontinuity in pressure where $\partial p/\partial t$ was initially largest.

(d) After shock wave has formed.

Figure 24. Schematic of large-amplitude continuous waves at increasing distances of propagation, showing pressure changes as a function of time.

would coexist simultaneously at the same place—an obvious impossibility. Instead, the shock continues to propagate with an excess velocity which is nominally zero in a continuous, symmetrical waveform, and the region where $\partial p/\partial t$ is negative becomes less steep (eq. (18) still applies in this region). In particular, the element either at, or just behind, the peak marked "A" in figure 24(d), continues to propagate with a velocity given by equation (18) and so coalesces with the shock wave. Thus an element, such as point A, that has a pressure just more than the pressure in the shock wave catches up to the shock because of its greater velocity to produce a more rapid reduction in pressure amplitude than would be predicted by linear absorption

or dissipation mechanisms. Similar processes occur on the low pressure side of the shock, with the result that the magnitude of the shock is eroded from both sides simultaneously. This enhanced rate of dissipation of acoustic energy is caused by the enhanced rate of conversion of this energy into heat through thermal and viscous processes associated with the very large thermal gradients across the shock front.

We have so far in this section described the nonlinear distortion of a sound wave in terms of its waveform as a function of time. An equally valid approach is to consider the change in its spectrum. The spectrum of an initially sinusoidal wave (fig. 24(a)) is a single frequency f_1 having a wavelength λ_1 given by $\lambda_1 = c_o/f_1$. As the wave propagates and progressively distorts, in the limit into a train of triangular waveforms, as shown by the solid line waveform in figure 24(d), the initial single-frequency spectrum f_1 changes to include higher harmonics nf_1 (where n is an integer). Before shocks have formed (figs. 24(a) and (b)), the amplitude of the second harmonic in a spherically spreading wave grows at a rate given by (ref. 55)

$$\frac{dp_2}{dx} = A_2 (p_1)_0^2 \left(\frac{x_0}{x}\right)^2 e^{2\alpha_1 (x - x_0)} - \frac{p_2}{x} - \alpha_2 p_2 \tag{19}$$

In equation (19) the first term represents the growth of the second harmonic from the fundamental at a rate depending (ref. 56) on the square of the fundamental amplitude $(p_1)_0$ which is itself subject to geometrical spreading (x_0/x) and to a small-amplitude attenuation coefficient α_1. The second term p_2/x represents the geometrical spreading of the second harmonic with distance of propagation, and the third term its dissipative attenuation. Expressions similar to equation (19) can be developed for higher harmonics and integrated to obtain the amplitudes of each harmonic as a function of the distance of propagation. These details are beyond the scope of this summary and interested readers are referred to references 54 and 55. In equation (19) for a spherically spreading finite-amplitude wave, the rate of generation of the second harmonic decreases as x^{-2}, more rapidly than the magnitude of either the first or the second harmonic, both of which decrease as x^{-1}.

Large-Amplitude Pulses

The large-amplitude waves considered so far have been assumed to be repetitive and symmetrical. Many large-amplitude waves are, however, transient pulses such as blasts, gun shots, or sonic booms. In these waves the initial pressure disturbance, usually an increase in pressure, propagates into undisturbed air (fig. 25(a)). Subsequent parts of the disturbance can have various forms such as a decaying oscillatory waveform or after one or two half-cycles a more or less immediate return to a relatively undisturbed state.

As before, nonlinear distortion occurs due to the finite magnitude of the particle velocity u, as described by equation (18). The pulse becomes more distorted during propagation, and at some distance a shock may form in the pulse where the pressure rise time $\partial p/\partial t$ was initially steepest. For simplicity of description (and this is often the case of practice), we assume that this is at the beginning of the pressure disturbance. The zero crossings of the pressure pulse, up to this time (fig. 25(b)) travel with the small-amplitude sound speed c_o. Once a shock has formed, it propagates with a velocity that is the mean of that associated with conditions immediately ahead of and behind it. This excess velocity is in the direction of

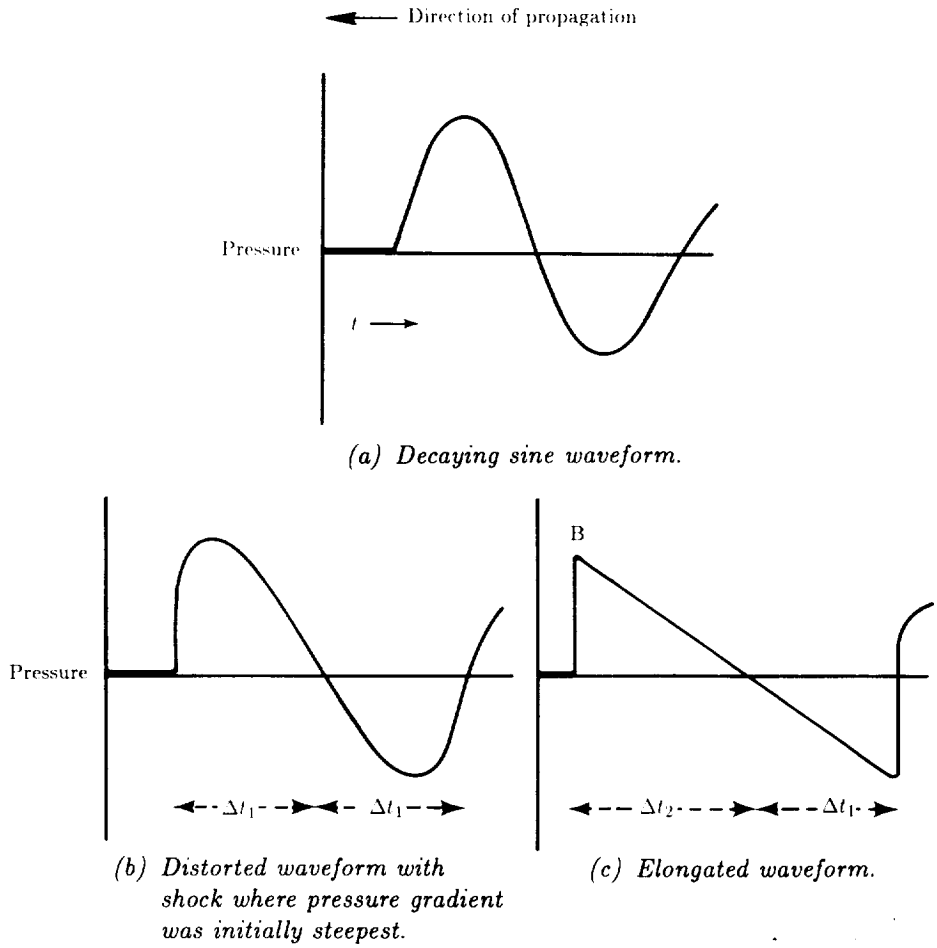

(a) Decaying sine waveform.

(b) Distorted waveform with shock where pressure gradient was initially steepest.

(c) Elongated waveform.

Figure 25. Schematic of a large-amplitude sound pulse at increasing distances of propagation showing pressure changes as a function of time.

propagation and causes the first half-cycle of the pulse to elongate as the pulse continues to propagate—later half-cycles of the pulse remain of constant duration Δt_1, until nonlinear distortion causes further and often unsymmetrical shocks to form in those parts of the pulse. This is illustrated in figure 25(c) where one notes that the first half-cycle has a duration Δt_2 that is longer than that of the second half-cycle of duration Δt_1. If we denote the particle velocity of the first peak of the wave, B in figure 25(c), by $u_{\max}$, then the velocity of the head shock for a pulse is given by

$$c = c_o + \frac{\gamma + 1}{4} u_{\max} \tag{20}$$

The second most likely place for a shock to form is at the end of the second half-cycle of the pulse, as shown in figure 25(c). This represents a typical N-wave, so-called because of its shape. Given the asymmetry of pressure usually associated with this tail shock, its mean velocity in the direction of propagation of the pulse is less than that of the zero crossings. Thus the head shock travels faster than c_o and the tail

shock slower, so that both contribute to the lengthening of the pulse, or equivalently an increased time duration between the head and tail shocks. The lengthening of a pulse traveling into undisturbed air is a feature that does not occur during the propagation of large-amplitude continuous waves even when shocks are present.

In terms of the spectrum of the pulse, this lengthening process represents a shift in the sound energy to lower frequencies as propagation proceeds. This is in sharp contrast to the shift in sound energy to higher frequencies as described earlier that is related to the nonlinear distortion from an initially more or less sinusoidal waveform to one having a more nearly triangular or saw-toothed shape—a process that occurs both in pulses and in continuous waves of large amplitude.

Sonic Booms

An important type of large-amplitude acoustic pulse is that caused by a body traveling faster than the local speed of sound (refs. 57 and 58). Of particular interest is the sonic boom caused by an aircraft flying supersonically. Because the aircraft is flying supersonically, pressure discontinuities (shock waves) are produced instantaneously at the source and are not produced by waveform distortion during propagation. Booms recorded on the ground from high flying aircraft are often good approximations to N-waves. If the aircraft is long or is flying sufficiently high for the N-wave to lengthen appreciably during propagation over a large distance, the head and tail shocks can be heard as two separate events between which there is a brief period of quiet. Reference 59 quotes results from several NASA Technical Notes showing that the time between head and tail shocks for a fighter aircraft increases systematically from about 50 msec to about 90 msec during propagation from 20 m to 3 km.

These authors (ref. 59) and others show that the pulse shape measured near a supersonic aircraft is not a simple N-wave but exhibits fine structure relating to the details of the aircraft's cross-sectional area and lift distribution. Each increase in cross-sectional area, such as the nose or leading edge of wing, produces its own head shock; and each decrease, such as the back end of the fuselage or wing, its own tail shock. However, following the same principles of propagation as described earlier, each head shock that starts out situated part way along the pulse, for example, that due to the leading edge of the wing, propagates faster than the local speed of sound, and makes its way forward in the pulse as the whole pulse propagates away from the aircraft. At a sufficient distance, all such intermediate head shocks coalesce with the frontmost head shock to produce a single head shock representing the beginning of the N-wave. Similarly all the intermediate tail shocks, traveling more slowly than the local speed of sound eventually coalesce into a single tail shock representing the end of the N-wave.

It is sometimes observed that sonic boom waveforms differ noticeably from well-defined N-waves. These discrepancies usually occur close to the head and tail shocks and rarely in the intermediate parts of the waveform. The peaks of the waveform may be very significantly rounded in shape; at other times the peaks appear to have sharp spikes superimposed on them. These effects are caused by propagation of the waves through turbulence and by refractive effects that can cause focusing or defocusing of the N-wave pulses at particular measuring locations. Focusing and defocusing of the waves can also be caused by aircraft maneuvers such as acceleration in straight

flight or turns. These factors have been studied by numerous workers and the reader should consult the literature for details (refs. 60–63).

Standards

The various sound propagation mechanisms described in the earlier sections of this chapter have all been studied and quantified by means of measurements. In some cases the measuring instruments used and methods of calculation or theories developed for these phenomena have been agreed upon and are now embodied in a number of national or international standards. A few of these standards are specific to noise from aircraft, but most are of more general application and relate to acoustical measurements of sound from almost any type of source. Here we can merely comment briefly on a number of these standards because standards are carefully developed precise documents, and anyone wishing to use a procedure described in a standard should refer to the standard itself.

The standard ANSI S1.13–1971 (R1986) (ref. 64) provides guidelines for the measurements of many different types of sound in various situations. A new standard is being developed to address specifically the special problems of measurement of sound pressure levels outdoors. The standards IEC 651(1979) (ref. 65) and ANSI S1.4–1983 (ref. 66) deal with the basic sound measurement system and specify frequency weighting and time constants. The standards ANSI S1.6–1984 (ref. 67), ANSI S1.8–1969 (R1974) (ref. 68) and ISO 1683–1983 (ref. 69) attempt to provide uniformity in the reporting of results. The latter two standards differ over the reference quantities to be used for vibratory velocity and acceleration. A major revision of ANSI S1.11 has been undertaken and the revised version, ANSI S1.11–1976 (R1986) (ref. 70), includes specifications for both digital and analog filters. The standard ANSI S1.26–1978 (ref. 5) relates directly to the propagation phenomenon described earlier in this chapter. It is currently undergoing revision to allow for more realistic values of attenuation at low frequencies and to include methods for calculating the attenuation of bands of noise and for calculating attenuation along a propagation path where the atmospheric properties change, for example, with altitude. Several other standards relate to specific types of aircraft operation under specific circumstances: SAE AIR-923 (ref. 71), SAE AIR-1672B (ref. 72), ISO 2249-1973 (ref. 73), and IEC 561(1976) (ref. 74).

The use of standard measurement procedures and methods of calculation has the obvious advantage of uniformity and of increasing the comparability of measurements made at different locations and times. However, in the subject of atmospheric sound propagation our collective knowledge of the several mechanisms involved and how they interact has advanced rapidly. For this reason, the discussion of some of the mechanisms in this chapter is based on new understanding that was not available at the time some of the standards were written.

References

1. Hunt, Frederick V.: *Origins in Acoustics.* Yale Univ. Press, 1978.
2. Lenihan, J. M. A.: Mersenne and Gassendi. *Acustica,* vol. 1, no. 2, 1951, pp. 96–99.
3. Piercy, J. E.; Embleton, T. F. W.; and Sutherland, L. C.: Review of Noise Propagation in the Atmosphere. *J. Acoust. Soc. America,* vol. 61, no. 6, June 1977, pp. 1403–1418.
4. Embleton, T. F. W.: Sound Propagation Outdoors—Improved Prediction Schemes for the 80's. *Noise Control Eng.,* vol. 18, no. 1, Jan.–Feb. 1982, pp. 30–39.

5. *American National Standard Method for the Calculation of the Absorption of Sound by the Atmosphere.* ANSI S1.26-1978 (ASA 23-1978), American Natl. Standards Inst., Inc., June 23, 1978.
6. Bass, H. E.; Sutherland, L. C.; Piercy, Joe; and Evans, Landon: Absorption of Sound by the Atmosphere. *Physical Acoustics, Volume XVII,* Warren P. Mason and R. N. Thurston, eds., Academic Press, Inc., 1984, pp. 145–232.
7. *Standard Values of Atmospheric Absorption as a Function of Temperature and Humidity for Use in Evaluating Aircraft Flyover Noise.* ARP 866A, Soc. Automot. Eng., Aug. 1964.
8. Zuckerwar, Allan J.; and Meredith, Roger W.: Low-Frequency Absorption of Sound in Air. *J. Acoust. Soc. America,* vol. 78, no. 3, Sept. 1985, pp. 946–955.
9. Wait, James R.: *Electromagnetic Waves in Stratified Media, Revised Edition Including Supplemented Material.* Pergamon Press Inc., c.1970.
10. Dickinson, P. J.; and Doak, P. E.: Measurements of the Normal Acoustic Impedance of Ground Surfaces. *J. Sound & Vib.,* vol. 13, no. 3, Nov. 1970, pp. 309–322.
11. Embleton, T. F. W.; Piercy, J. E.; and Olson, N.: Outdoor Sound Propagation Over Ground of Finite Impedance. *J. Acoust. Soc. America,* vol. 59, no. 2, Feb. 1976, pp. 267–277.
12. Zuckerwar, Allan J.: Acoustic Ground Impedance Meter. *J. Acoust. Soc. America,* vol. 73, no. 6, June 1983, pp. 2180–2186.
13. Allard, Jean F.; and Sieben, Benita: Measurements of Acoustic Impedance in a Free Field With Two Microphones and a Spectrum Analyzer. *J. Acoust. Soc. America,* vol. 77, no. 4, Apr. 1985, pp. 1617–1618.
14. Daigle, G. A.; and Stinson, Michael R.: Impedance of Grass-Covered Ground at Low Frequencies Measured Using a Phase Difference Technique. *J. Acoust. Soc. America,* vol. 81, no. 1, Jan. 1987, pp. 62–68.
15. Chessell, C. I.: Propagation of Noise Along a Finite Impedance Boundary. *J. Acoust. Soc. America,* vol. 62, no. 4, Oct. 1977, pp. 825–834.
16. Delany, M. E.; and Bazley, E. N.: Acoustical Properties of Fibrous Absorbent Materials. *Appl. Acoust.,* vol. 3, no. 2, Apr. 1970, pp. 105–116.
17. Embleton, T. F. W.; Piercy, J. E.; and Daigle, G. A.: Effective Flow Resistivity of Ground Surfaces Determined by Acoustical Measurements. *J. Acoust. Soc. America,* vol. 74, no. 4, Oct. 1983, pp. 1239–1244.
18. Attenborough, K.: Acoustical Impedance Models for Outdoor Ground Surfaces. *J. Sound & Vib.,* vol. 99, no. 4, Apr. 22, 1985, pp. 521–544.
19. Nicolas, J.; Berry, J.-L.; and Daigle, G. A.: Propagation of Sound Above a Finite Layer of Snow. *J. Acoust. Soc. America,* vol. 77, no. 1, Jan. 1985, pp. 67–73.
20. Naghieh, M.; and Hayek, Sabih I.: Diffraction of a Point Source by Two Impedance Covered Half-Planes. *J. Acoust. Soc. America,* vol. 69, no. 3, Mar. 1981, pp. 629–637.
21. Rasmussen, K. B.: A Note on the Calculation of Sound Propagation Over Impedance Jumps and Screens. *J. Sound & Vib.,* vol. 84, no. 4, Oct. 22, 1982, pp. 598–602.
22. De Jong, B. A.; Moerkerken, A.; and Van der Toorn, J. D.: Propagation of Sound Over Grassland and Over an Earth Barrier. *J. Sound & Vib.,* vol. 86, no. 1, Jan. 8, 1983, pp. 23–46.
23. Koers, Peter: Diffraction by an Absorbing Barrier or by an Impedance Transition. *Noise Control: The International Scene, Proceedings—Inter-Noise 83, Volume 1,* Inst. of Acoustics (Edinburgh, U.K.), c.1983, pp. 311–314.
24. Daigle, G. A.; Nicolas, J.; and Berry, J.-L.: Propagation of Noise Above Ground Having an Impedance Discontinuity. *J. Acoust. Soc. America,* vol. 77, no. 1, Jan. 1985, pp. 127–138.
25. Embleton, T. F. W.; Thiessen, G. J.; and Piercy, J. E.: Propagation in an Inversion and Reflections at the Ground. *J. Acoust. Soc. America,* vol. 59, no. 2, Feb. 1976, pp. 278–282.
26. Parkin, P. H.; and Scholes, W. E.: The Horizontal Propagation of Sound From a Jet Engine Close to the Ground, at Hatfield. *J. Sound & Vib.,* vol. 2, no. 4, Oct. 1965, pp. 353–374.
27. Hidaka, Takayuki; Kageyama, Kenji; and Masuda, Sadahiro: Sound Propagation in the Rest Atmosphere With Linear Sound Velocity Profile. *J. Acoust. Soc. Japan (E),* vol. 6, no. 2, Apr. 1985, pp. 117–125.
28. Raspet, R.; Lee, S. W.; Kuester, E.; Chang, D. C.; Richards, W. F.; Gilbert, R.; and Bong, N.: Fast-Field Program for Sound Propagation in a Layered Atmosphere Above an Impedance Ground. *J. Acoust. Soc. America,* vol. 77, no. 2, Feb. 1985, pp. 345–352.

29. Lee, S. W.; Bong, N.; Richards, W. F.; and Raspet, Richard: Impedance Formulation of the Fast Field Program for Acoustic Wave Propagation in the Atmosphere. *J. Acoust. Soc. America,* vol. 79, no. 3, Mar. 1986, pp. 628–634.
30. Pierce, Allan D.: *Acoustics—An Introduction to Its Physical Principles and Applications.* McGraw-Hill Book Co., c.1981.
31. Daigle, G. A.; Embleton, T. F. W.; and Piercy, J. E.: Propagation of Sound in the Presence of Gradients and Turbulence Near the Ground. *J. Acoust. Soc. America,* vol. 79, no. 3, Mar. 1986, pp. 613–627.
32. Tatarski, V. I. (R. A. Silverman, transl.): *Wave Propagation in a Turbulent Medium.* McGraw-Hill Book Co., Inc., 1961.
33. Johnson, Mark A.; Raspet, Richard; and Bobak, Michael T.: A Turbulence Model for Sound Propagation From an Elevated Source Above Level Ground. *J. Acoust. Soc. America,* vol. 81, no. 3, Mar. 1987, pp. 638–646.
34. Daigle, G. A.; Piercy, J. E.; and Embleton, T. F. W.: Line-of-Sight Propagation Through Atmospheric Turbulence Near the Ground. *J. Acoust. Soc. America,* vol. 74, no. 5, Nov. 1983, pp. 1505–1513.
35. Brown, Edmund H.; and Hall, Freeman F., Jr.: Advances in Atmospheric Acoustics. *Rev. Geophys. & Space Phys.,* vol. 16, no. 1, Feb. 1978, pp. 47–110.
36. Brown, E. H.; and Clifford, S. F.: On the Attenuation of Sound by Turbulence. *J. Acoust. Soc. America,* vol. 60, no. 4, Oct. 1976, pp. 788–794.
37. Wenzel, Alan R.: Radiation and Attenuation of Waves in a Random Medium. *J. Acoust. Soc. America,* vol. 71, no. 1, Jan. 1982, pp. 26–35.
38. Daigle, G. A.: Effects of Atmospheric Turbulence on the Interference of Sound Waves Above a Finite Impedance Boundary. *J. Acoust. Soc. America,* vol. 65, no. 1, Jan. 1979, pp. 45–49.
39. Clifford, Steven F.; and Lataitis, Richard J.: Turbulence Effects on Acoustic Wave Propagation Over a Smooth Surface. *J. Acoust. Soc. America,* vol. 73, no. 5, May 1983, pp. 1545–1550.
40. Hidaka, T.; Kageyama, K.; and Masuda, S.: Fluctuation of Spherical Wave Propagating Over a Ground Through Atmospheric Turbulence. *J. Acoust. Soc. Japan (E),* vol. 6, no. 2, Apr. 1985, pp. 247–256.
41. Daigle, G. A.: Diffraction of Sound by a Noise Barrier in the Presence of Atmospheric Turbulence. *J. Acoust. Soc. America,* vol. 71, no. 4, Apr. 1982, pp. 847–854.
42. Keller, Joseph B.: Geometrical Theory of Diffraction. *J. Opt. Soc. America,* vol. 52, no. 2, Feb. 1962, pp. 116–130.
43. Elmore, William C.; and Heald, Mark A.: *Physics of Waves.* McGraw-Hill Book Co., c.1969.
44. Born, Max; and Wolf, Emil: *Principles of Optics,* Fourth ed. Pergamon Press Inc., 1970.
45. Isei, T.; Embleton, T. F. W.; and Piercy, J. E.: Noise Reduction by Barriers on Finite Impedance Ground. *J. Acoust. Soc. America,* vol. 67, no. 1, Jan. 1980, pp. 46-58.
46. Pierce, Allan D.: Diffraction of Sound Around Corners and Over Wide Barriers. *J. Acoust. Soc. America,* vol. 55, no. 5, May 1974, pp. 941–955.
47. Fujiwara, K.; Ando, Y.; and Maekawa, Z.: Noise Control by Barriers—Part I: Noise Reduction by a Thick Barrier. *Appl. Acoust.,* vol. 10, no. 2, Apr. 1977, pp. 147–159.
48. Maekawa, Z.: Noise Reduction by Screens. *Appl. Acoust.,* vol. 1, no. 3, July 1968, pp. 157–173.
49. Daigle, G. A.; and Embleton, T. F. W.: Diffraction of Sound Over Curved Ground. *J. Acoust. Soc. America,* vol. 79, suppl. no. 1, Spring 1986, p. S20.
50. Pierce, Allan D.; Main, Geoffrey L.; and Kearns, James A.: Curved Surface Diffraction Theory Derived and Extended Using the Method of Matched Asymptotic Expansions. *J. Acoust. Soc. America,* vol. 79, suppl. no. 1, Spring 1986, pp. S30–S31.
51. Berry, Alain; and Daigle, G. A.: Propagation of Sound Above a Curved Surface. *J. Acoust. Soc. America,* vol. 81, suppl. no. 1, Spring 1987, p. S97.
52. Berthelot, Yves H.; Kearns, James A.; Pierce, Allan D.; and Main, Geoffrey L.: Experimental Investigation of the Diffraction of Sound by a Curved Surface of Finite Impedance. *J. Acoust. Soc. America,* vol. 81, suppl. no. 1, Spring 1987, p. S97.
53. Blackstock, David T.: Connection Between the Fay and Fubini Solutions for Plane Sound Waves of Finite Amplitude. *J. Acoust. Soc. America,* vol. 39, no. 6, June 1966, pp. 1019–1026.
54. Blackstock, David T.: Nonlinear Behavior of Sound Waves. *12th International Congress on Acoustics.* Canadian Acoustical Assoc., July 1986, Plenary 3.

55. Pernet, D. F.; and Payne, R. C.: Non-Linear Propagation of Signals in Air. *J. Sound & Vib.*, vol. 17, no. 3, Aug. 8, 1971, pp. 383–396.
56. Thuras, A. L.; Jenkins, R. T.; and O'Neil, H. T.: Extraneous Frequencies Generated in Air Carrying Intense Sound Waves. *J. Acoust. Soc. America*, vol. 6, no. 3, Jan. 1935, pp. 173–180.
57. *Proceedings of the Sonic Boom Symposium. J. Acoust. Soc. America*,, vol. 39, no. 5, pt. 2, May 1966, pp. S1–S80.
58. *Sonic Boom Symposium. J. Acoust. Soc. America*, vol. 51, no. 2, (pt. 3), Feb. 1972.
59. Carlson, Harry W.; Mack, Robert J.; and Morris, Odell A.: Sonic-Boom Pressure-Field Estimation Techniques. *J. Acoust. Soc. America*, vol. 39, no. 5, pt. 2, May 1966, pp. S10–S18.
60. Kane, E. J.: Some Effects of the Nonuniform Atmosphere on the Propagation of Sonic Booms. *J. Acoust. Soc. America*, vol. 39, no. 5, pt. 2, May 1966, pp. S26–S30.
61. Maglieri, Domenic J.: Some Effects of Airplane Operations and the Atmosphere on Sonic-Boom Signatures. *J. Acoust. Soc. America*, vol. 39, no. 5, pt. 2, May 1966, pp. S36–S42.
62. Pierce, Allan D.; and Maglieri, Domenic J.: Effects of Atmospheric Irregularities on Sonic-Boom Propagation. *J. Acoust. Soc. America*, vol. 51, no. 2, pt. 3, Feb. 1972, pp. 702–721.
63. Wanner, Jean-Claude L.; Vallee, Jacques; Vivier, Claude; and Thery, Claude: Theoretical and Experimental Studies of the Focus of Sonic Booms. *J. Acoust. Soc. America*, vol. 52, no. 1, pt. 1, July 1972, pp. 13–32.
64. *American National Standard Methods for the Measurement of Sound Pressure Levels.* ANSI S1.13-1971 (R1976) (Partial revision of S1.2-1962 (R1971)), American National Standards Inst., Inc., July 14, 1971.
65. *Sound Level Meters, First ed.* Publ. 651, International Electrotechnical Commission, 1979.
66. *American National Standard Specification for Sound Level Meters.* ANSI S1.4-1983 (Revision of S1.4-1971) (ASA 47-1983), Acoustical Soc. America, 1983.
67. *American National Standard Preferred Frequencies, Frequency Levels, and Band Numbers for Acoustical Measurements.* ANSI S1.6-1984 (Rev. of S1.6-1967 (R1976)) (ASA 53-1984), Acoustical Soc. of America, 1984.
68. *American National Standard Preferred Reference Quantities for Acoustical Levels.* ANSI S1.8-1969 (R1974) (Corrected edition), American National Standards Inst., Inc., Feb. 24, 1969.
69. *Acoustics—Preferred Reference Quantities for Acoustic Levels.* ISO 1683-1983 (E), International Organization of Standards, 1983.
70. *American National Standard Specification for Octave-Band and Fractional-Octave-Band Analog and Digital Filters.* ANSI S1.11-1986 (ASA 65-1986) (Rev. of ANSI S1.11-1966 (R1976)), Acoustical Soc. of America, 1986.
71. *Method for Calculating the Attenuation of Aircraft Ground to Ground Noise Propagation During Takeoff and Landing.* AIR 923, Soc. Automotive Engineers, Mar. 1, 1968.
72. *Practical Methods To Obtain Free-Field Sound Pressure Levels From Acoustical Measurements Over Ground Surfaces.* AIR 1672B, Soc. Automotive Engineers, Inc., June 1983.
73. *Acoustics—Description and Measurement of Physical Properties of Sonic Booms.* ISO 2249-1973 (E), International Organization of Standards, 1973.
74. *Electro-Acoustical Measuring Equipment for Aircraft Noise Certification, First ed.* Publ. 561, International Electrotechnical Commission, 1976.